NAVAL POSTGRADUATE SCHOOL
Monterey, California

THESIS

VERIFYING DIGITAL FILTER
INITIALIZATION IN A 3-DIMENSIONAL
COASTAL OCEAN MODEL

by

David E. Otis

March 1995

Thesis Advisor: Robert L. Haney

REPORT DOCUMENTATION PAGE

Form Approved OMB No. 0704-0188

1. AGENCY USE ONLY *(Leave blank)*	2. REPORT DATE March 1995	3. REPORT TYPE AND DATES COVERED Master's Thesis

4. TITLE AND SUBTITLE VERIFYING DIGITAL FILTER INITIALIZATION IN A 3-DIMENSIONAL COASTAL OCEAN MODEL

5. FUNDING NUMBERS

6. AUTHOR(S) LT David E. Otis

7. PERFORMING ORGANIZATION NAME(S) AND ADDRESS(ES)
Naval Postgraduate School
Monterey CA 93943-5000

8. PERFORMING ORGANIZATION REPORT NUMBER

9. SPONSORING/MONITORING AGENCY NAME(S) AND ADDRESS(ES)

10. SPONSORING/MONITORING AGENCY REPORT NUMBER

11. SUPPLEMENTARY NOTES The views expressed in this thesis are those of the author and do not reflect the official policy or position of the Department of Defense or the U.S. Government.

12a. DISTRIBUTION/AVAILABILITY STATEMENT
Approved for public release; distribution is unlimited.

12b. DISTRIBUTION CODE

13. ABSTRACT *(maximum 200 words)*

A primitive equation model is used to simulate mesoscale ocean variability to verify the digital filter initialization (DFI) method of Lynch and Huang. The model is initialized with two different analytic density fields, a linear Rossby wave and a baroclinically unstable flow, and then integrated forward to produce control runs. Both simulations resulted in measurable ageostrophic currents and vertical motions. The density field at the end of the control runs was extracted and used by DFI to regenerate the control currents. Combinations of different DFI integration times and repeated DFI passes, were used. The normalized rms error between the vertical velocities from the control runs and from DFI, showed that the 12-hr and 3 pass combination had the greatest accuracy. The normalized error was less than 0.15, except near the bottom of the domain and also at the surface for the shallow baroclinically unstable flow. This was attributed to the neglect of friction in the DFI processes, and to somewhat poor vertical resolution near the surface for the unstable case. The errors were small enough to be confident that DFI accurately recovered the adiabatic, frictionless part of the control's currents.

14. SUBJECT TERMS Digital Filter Initialization, Secondary Circulation, Ageostrophic Currents

15. NUMBER OF PAGES 74

16. PRICE CODE

17. SECURITY CLASSIFICATION OF REPORT	18. SECURITY CLASSIFICATION OF THIS PAGE	19. SECURITY CLASSIFICATION OF ABSTRACT	20. LIMITATION OF ABSTRACT
Unclassified	Unclassified	Unclassified	UL

NSN 7540-01-280-5500

Standard Form 298 (Rev. 2-89)
Prescribed by ANSI Std. 239-18 298-102

Approved for public release; distribution is unlimited.

VERIFYING DIGITAL FILTER INITIALIZATION IN A 3-DIMENSIONAL COASTAL OCEAN MODEL

David E. Otis
Lieutenant, United States Navy
B.S., Michigan State University, 1979
B.S., Michigan State University, 1985

Submitted in partial fulfillment
of the requirements for the degree of

MASTER OF SCIENCE IN METEOROLOGY AND PHYSICAL OCEANOGRAPHY

from the
NAVAL POSTGRADUATE SCHOOL
March 1995

Author: David E. Otis
David E. Otis

Approved by: Robert L. Haney
Robert L. Haney, Thesis Advisor

R. T. Williams
R. T. Williams, Second Reader

Robert L. Haney
Robert L. Haney, Chairman
Department of Meteorology

ABSTRACT

A primitive equation model is used to simulate mesoscale ocean variability to verify the digital filter initialization (DFI) method of Lynch and Huang. The model is initialized with two different analytic density fields, a linear Rossby wave and a baroclinically unstable flow, and then integrated forward to produce control runs. Both simulations resulted in measurable ageostrophic currents and vertical motions. The density field at the end of the control runs was extracted and used by DFI to regenerate the control currents. Combinations of different DFI integration times and repeated DFI passes, were used. The normalized rms error between the vertical velocities from the control runs and from DFI, showed that the 12-hr and 3 pass combination had the greatest accuracy. The normalized error was less than 0.15, except near the bottom of the domain and also at the surface for the shallow baroclinically unstable flow. This was attributed to the neglect of friction in the DFI processes, and to somewhat poor vertical resolution near the surface for the unstable case. The errors were small enough to be confident that DFI accurately recovered the adiabatic, frictionless part of the control's currents.

TABLE OF CONTENTS

I. INTRODUCTION 1
A. BACKGROUND 2
1. Methods to Determine Divergence 2
a. Methods Based on Dynamical and Thermodynamical Equations 2
b. Drifting Buoys 4
c. Tracking Nutrients and Chlorophyll . 5
d. DFI in the Atmosphere 6
B. OBJECTIVE 7
C. MODEL AND METHODS 7

II. RESULTS 11
A. CONTROL RUN - LINEAR ROSSBY WAVES 11
1. Setup 11
2. Control Simulation 13
3. DFI Verification 13
B. BAROCLINIC UNSTABLE MEAN FLOW - RUN TO FINITE AMPLITUDE 32
1. Setup 32
2. Control Simulation 34
3. DFI Verification 37

III. DISCUSSION AND CONCLUSIONS 55

LIST OF REFERENCES 59

INITIAL DISTRIBUTION LIST 61

ACKNOWLEDGMENT

The author would like to thank Prof. Haney for his guidance and patient direction throughout the course of this study. The gratitude of the author also goes to Bob Hale for his assistance and help with the computer simulation.

I. INTRODUCTION

In recent years the U.S. Navy has shifted its attention and operation from open-ocean warfare, to expeditionary roles in the "littoral" environment of the coastlines of the world. The new emphasis was first set forth in the U.S. Navy's white paper, "...From the Sea," (O'Keefe et al. 1992) and amplified in the follow-on white paper, "Forward...From the Sea" (Dalton et al. 1994). The needs of a naval expeditionary force are different from those of a deep water force. Anti-Submarine warfare becomes a difficult challenge in the coastal waters, where sound propagation is very complex and not modeled very well. Mine warfare becomes increasingly important with a desire for an increased ability to detect moored mines, and a complex environment that poses unique challenges for all forces that operate within these areas. This focus on the littoral has caused increased attention on numerical coastal prediction models with a desire to increase the accuracy of their forecasts.

One direct method to raise the accuracy of the product is to increase the accuracy of the initial conditions. This goal could be satisfied by the digital filter initialization (DFI) method of Lynch and Huang (1992). DFI would accomplish this by reducing the gravity wave (high frequency) noise at the start of a model forecast cycle. Gravity wave noise is a result of the imbalances in the horizontal equations of motion. By removing these imbalances from the model additional shocks, from the imbalances between the model dynamics and the vertical circulation, could be eliminated. The initialization procedure must also emulate the effects of the geostrophic adjustment process, so that the initialized currents have a divergent component, resulting in vertical motions.

Horizontal velocities can be measured directly with

current meters, drifting buoys, etc. However, the accuracy of these measurements is not sufficient to directly determine the vertical velocity through mass continuity. The difficulty with accurately initializing a 3-dimensional circulation model therefore lies with how the vertical velocities are determined. These must be indirectly inferred or diagnosed with the accuracy depending upon the assumptions, methods used, and the manner the data were collected.

Many operational weather prediction centers, including the Fleet Numerical Oceanography Center (FNMOC), use nonlinear normal mode initialization (NNMI) to begin their forecast models. However, Lynch and Huang (1992) recently showed that DFI is equivalent (if not superior) to NNMI and is far easier to apply.

The purpose of this thesis is to validate the DFI method within the context of a coastal ocean prediction model. If the DFI method is quantitatively validated, it can be used as an initialization method for numerical ocean prediction models. It can also be utilized to diagnose the vertical circulation and ageostrophic velocity from observed data sets and thereby used in dynamical studies.

A. BACKGROUND

1. Methods to Determine Divergence

Several methods have been employed to diagnose the divergent component of the current and its associated vertical velocity. The following is a brief review of a selection of several methods used to reveal the vertical velocity structure.

a. Methods Based on Dynamical and Thermodynamical Equations

In his paper Strass (1994) reviewed a set of numerical methods. He analyzed and ranked the isopycnic advection equation, the vorticity advection equation and the

Q-vector version of the omega equation, as they were applied to estimate the mesoscale distribution of vertical motions. Strass used the mesoscale term to refer to scales as small as the Rossby radius of deformation, which is typically on the order of 25 km. The methods were tested to determine how their computed vertical velocities compared to "observed", and if the w velocity was consistent with the model variables. "Observed" values were determined from controlled numerical solutions. The results showed that the Q-vector method was best for diagnosis of the horizontal pattern of vertical motion. Nevertheless, when the integration time advanced causing the vertical velocity to have its strongest variance, the coherence decreased for wavelengths less than 10 km (high wavenumbers) (Strass 1994).

Advection of vorticity was found to be the second best method for predicting the model's vertical velocity. However, here too, was a drop of coherence, at even higher wavenumbers than those found in the Q-vector method, (beginning at 30 km). Additionally a looser relationship to the modeled w, was found concerning the phase.

Strass (1994) found the least accurate model was the isopycnic advection model, which diagnoses w from a steady state thermodynamic equation (assuming the horizontal and vertical advection balanced). It reproduced the large scale distribution of vertical motion, but it was deficient in the smaller scales, as no individual upwelling or downwelling areas were correctly identified. In fact there was a progressive phase error over time that settled near 180 degrees out of phase (i.e., upwelling predicted for actual downwelling and vice versa). The overall correlation was therefore lower than the other two methods. The stationarity assumption becomes fatal for the oceanic synoptic scale.

Vertical velocity distribution patterns were best predicted by the Q-vectors of the quasi-geostrophic (QG) omega

equation, and the amplitude had an error of only a few tens of percent. However, to convert the divergence from the voriticity advection, or the convergence from the Q-vector, or the Q-vector potential into vertical motion, a scaling factor had to be used (Strass 1994). This result was expected since the Q-vector form of the QG omega equation is known to be the more accurate method (Holton 1992). The QG omega equation is derived from consistent vorticity and thermodynamic equations, with no assumptions of steady state. It is however, only valid for QG motions, i.e., those scales of motions for which the Rossby number is small.

b. Drifting Buoys

Several studies have used drifting buoys to directly find divergence and indirectly imply vertical motion. Swenson et al. (1988) used mixed layer drifters' trajectories and temperature measurements to arrive at the vertical velocity. They did not estimate divergence directly from the horizontal component of the flow, but rather indirectly from the vorticity budget. This required accurate estimations of the relative vorticity, which allowed the time derivatives of the buoys motion to be calculated (Swenson et al. 1988). The short comings of this were: that the estimated relative vorticity was taken from a subjectively chosen cluster of buoys; and that analyzing their relative motions and resulting vorticity changes were done for only small scales (12-15 km).

Lagrangian drifters, satellite images, direct sampling and hydrographic surveys were used by Paduan and Niiler (1990), to track water parcels at a given depth in California coastal waters. From their movement, estimates of the vertical velocity were made. "To attach physical relevance to the velocity gradient estimated using the cluster method, required making the assumption that there exists a separation in scales between cluster-scale and sub-cluster scale motions" (Paduan, Niiler 1990). They used the shallow

water approximation, and assumed that the wind driven curl effects were not important in the well-mixed layer. Nevertheless, they did allow Ekman transport. The direct estimates of divergence were unreliable and suggested a measure of uncertainty in the cluster method, when applied to determining divergence. This uncertainty exists particularly when small numbers of drifters are used, and when they spanned a maximum in the flow field. Relative vorticity was better estimated and used (with the vorticity budget) to locate areas of upwelling and downwelling.

Isopycnal RAFOS floats were used off Cape Hatteras by Bower (1989) to examine convergence and divergence. She estimated the horizontal divergence from the average rate of change of the absolute vorticity with time between the extremes of Gulf Stream meanders (Bower 1989). The change in time (Δt) was the time it took the float to traverse the segment over which the absolute vorticity was calculated. Uncertainties in the estimations of the divergence were a function of Δt and absolute vorticity. Float trajectories were used to estimate the sign of the horizontal divergence and the magnitudes of that divergence from the vorticity budget. The results were questionable due to uncertainties in estimating the vorticity associated with the lateral shear along a density surface. Thus they were only able to give upper and lower limits of divergence in the main thermocline (Bower 1989).

c. Tracking Nutrients and Chlorophyll

Beside the use of drifting buoys, the employment of satellite imagery, and sampling of the water have been applied to track nutrients, chlorophyll, etc., to estimate the vertical transportation in the ocean (Kadko et al. 1991). By tracking an isotope related to chlorophyll, Kadko et al. (1991) tried to determine how deep the chlorophyll would sink. They looked at the depth chlorophyll would sink to the half-

life of the isotope found at that depth. The isotope was assumed to combine with the chlorophyll at the surface and with its rapid half-life would only exist a short time as the chlorophyll began to sink. Chlorophyll was found at depths deeper than could be reached by the calculated sink rate. The presence of the isotope also showed that the chlorophyll was not being created by the phytoplankton at that depth. Kadko et al. (1991) concluded it must have been the result of rapid vertical transport with values estimated to be 5-20 m d^{-1} in the California current eddies.

Washburn et al. (1991) traced high concentrates of phytoplankton, and found phytoplankton at depths without enough light to grow and reproduce. They used the distribution of chlorophyll fluorescence, to give vertical resolution. Washburn et al. (1991) concluded that particle sinking rates were not the dominate process nor was the resuspension of bottom sediments that included phytoplankton. They resolved that to get chlorophyll at the observed depth, there had to be a subduction of surface waters. Washburn et al. (1991) also suggested, however that some vertical movement could be the result of mixing along sloping isopycnals. The vertical displacement based on the geostrophic flow on sloping density surfaces underestimated the vertical motions. This underestimation resulted from the calculations not going to the nearshore, where the isopycnals had the largest slope into the higher velocity nearshore flow (Washburn et al. 1991).

d. DFI in the Atmosphere

Lynch and Huang (1992), used the digital filter initialization (DFI) method to initialize the High Resolution Limited Area Model (HRLAM). The initialized fields represent dynamically balanced model variables with a realistic distribution of the ageostrophic flow and vertical velocity. HRLAM is a primitive equation forecast model of the atmosphere. A lowpass digital filter was applied to the time

series generated by a simple 3-hour forward and 3-hour backward model integration (6-hour total time span). This lowpass filtered time series, centered at the initial time, represented the dynamically balanced (initialized) fields of the model. Lynch and Huang (1992) also showed that this balanced field is equivalent to that obtained by the more complicated NNMI. A doubling of the total time span to 12 hours led to a damping of the meteorological modes. The forward and backward integrations were accomplished with the physics turned off, to allow no irreversible processes to be integrated backwards. The boundaries were held constant, but the fields inside were allowed to vary. Lynch and Huang (1992) showed that DFI eliminated initial gravity wave noise from the models used in atmospheric forecasting.

B. OBJECTIVE

The objective of this study is to prove that DFI can diagnose accurately the secondary circulations associated with quasi-geostrophic, and other higher order, dynamical balances. By illustrating the accuracy of the DFI method, it can then be applied with confidence, to better understand and predict mesoscale features in the littoral regions of the oceans.

C. MODEL AND METHODS

Following the approach of Strass (1994), the method used to test DFI was: to extract the density field from a controlled numerical model simulation; apply the DFI method to initialize the currents (including the vertical velocity); and finally verify the resulting initialized currents against the known currents from the control simulation. Two different simulations are carried out. One corresponded to linear Rossby waves and the other corresponded to a field of growing baroclinic disturbances typical of the coastal ocean. Starting a primitive equation numerical ocean model from an

initial condition of rest or geostrophic balance, causes the currents and mass fields to undergo relatively high frequency oscillations, as a part of the geostrophic adjustment process. When the initial condition is at a state of rest, the model has many more oscillations than when it is started from the geostrophic balance, and the adjustment process causes the geostrophic currents to be spun up. The ageostrophic currents are created by the geostrophic adjustment process when starting from the geostrophic balance case. The geostrophic/ageostrophic currents and the secondary circulation make up the "slow manifold" (Lorenz 1992) in the model. The "slow manifold" is that part of the oceanic state that may be considered determinably predictable. Lynch and Huang (1992) showed that a lowpass digital filter applied to the model's variables removed the high frequency oscillation (i.e., gravity waves), and returned the "slow manifold" at the analysis time. These variables were generated by short term forward and backward integrations that start from an uninitialized analysis.

The numerical model used is a multi-level, hydrostatic, nonlinear primitive equation model. The vertically integrated currents are nondivergent (i.e., "rigid lid"). There are 20 levels in the vertical, however the levels where w is calculated are staggered between the levels where u and v are calculated. For a given level the location of w is half a level lower than that for u and v. In the horizontal a 4 km grid spacing was used. The model is a cyclic zonal channel with insulated free-slip walls at the north and south boundaries, and a flat bottom. The model domain is 224 km from the east to the west and 224 km from the south to the north, with a total depth of 4000 m.

The DFI method used is similar to Lynch and Huang's (1992) approach. A time series of the model variables is generated by a short term forward and backward integration

from the initial time (Figure 1). The integrations are done without any forcing or friction. The resulting time-series is of length 2T, and a lowpass filter is then applied to it.

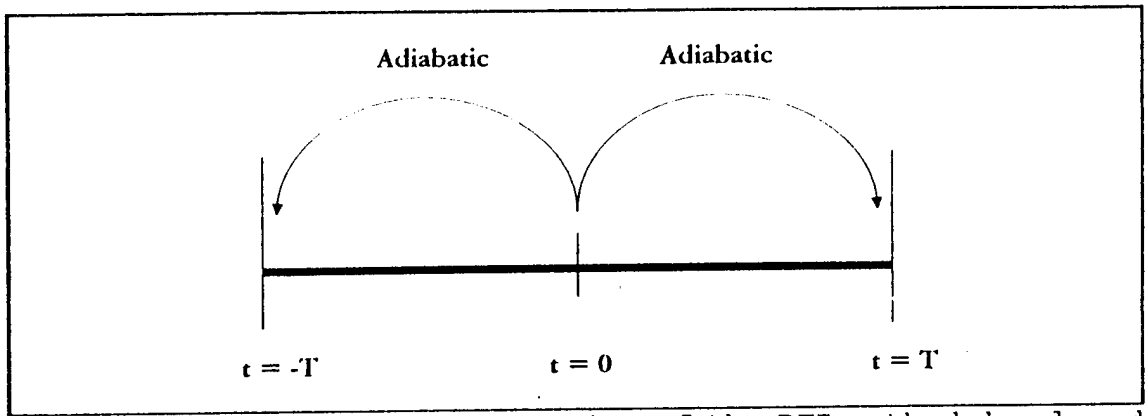

Figure 1. Schematic representation of the DFI method developed by Lynch and Huang 1992. Starting from a given initial condition, the model is integrated forward and backward.

Thus, if q represents any one of the model's variables, then the lowpass filtered value, corresponding to the dynamically balanced state at the time t = 0, is denoted by q_f, which given by:

$$q_f = \sum_{n=-N}^{n=N} h_n \, q_n \qquad (1)$$

Where h_n is the lowpass filter coefficient (Lynch and Huang 1992), and $q_n = q(n\Delta t)$ is the discrete value of the model variable at time $t = n\Delta t$, for $-T \leq t \leq T$ and $T = N\Delta t$.

Lynch and Huang (1992) showed that the integration and lowpass filter removed the high frequency noise and produced dynamically balanced model fields. These fields now have very little noise associated with them, when used to initialize the model and in the forward integration of the model's forecast. In this study the accuracy with which the DFI can diagnose the

known currents, by starting only with the known density field, is tested. In addition, the optimum value of the filter span T is determined and the usefulness of repeated initialization is also examined. A repeated initialization is one where the initialized variables, q_f, are used as initial conditions for subsequent forward and backward integration plus filter application. In fact several such repeated initialization steps were used to examine the resulting convergence to the known solution (control currents).

II. RESULTS

A. CONTROL RUN - LINEAR ROSSBY WAVES

1. Setup

The model was first initialized using DFI with a 12-hour forward and a 12-hour backward integration (2T = 24 hr total time span) and it was repeated 3 times. The DFI began at t = 0 with a large scale, small amplitude density disturbance with currents that were in geostrophic and hydrostatic balance. This density disturbance was defined in the model by the following equation:

$$dist = \left(\sin\left(6*\pi*\frac{x-\frac{xm}{2}}{xm}\right)\right)* \left(1+\cos\left(2*\pi*\frac{y-\frac{ym}{2}}{ym}\right)\right), \quad (2)$$

where xm and ym are both equal to 224 km, and are the x- and y- scales of the domain. It has a sine wave pattern with a wavenumber of 3 in the x-direction. Along the y-direction the density disturbance has a cosine pattern of wavenumber 1. This results in dist = 0 at the north (y = ym) and south (y = 0) boundaries, and a maximum in the center of the y-axis (y = ym/2). The disturbance in Equation (2) was then multiplied by a "form function" to give it a vertical profile that was constant from the surface to a depth of 37.5 m. Following that it underwent a smooth transition to an exponential profile beginning at 75 m. The exponential profile had a scale depth of 240 m.

This density disturbance was superimposed on a stratified zonal shear flow that was also in geostrophic and hydrostatic

balance. That current's density field was defined by the hyperbolic tangent of (y/y1), where y1 = ym*10^3. A nearly constant positive northward density gradient was created, such that the northern boundary of the model domain had a higher density than the southern boundary. The horizontal structure was also multiplied by the same z-dependent function as the density disturbance (constant in z above 37.5 m, and then a transition to an exponential function at 75 m, with a 240 m scale depth). The density gradient produced a nearly uniform zonal shear flow (with a corresponding exponential profile in z) that was centered in the middle of the y-axis.

The density disturbance and zonal flow were used in the DFI with a 12-hr integration time span and 3 repeated passes. From the DFI the density field and the associated currents were used to initialized the model. After the initialization, the model was integrated forward for 10 days, which allowed the large scale disturbance to evolve and propagate. The disturbance produced by Equation (2), evolved as a quasi-linear first baroclinic mode Rossby wave that was representative of a typical oceanic "slow mode". The model is on a f-plane and therefore, the "beta" effect was due to the weak northward gradient of the mean relative vorticity. The instantaneous density field was then extracted from the 10th day of the 10-day control integration. The day 10 density field was then used with the DFI procedure with the purpose of trying to recover the original day 10 (slightly nongeostrophic) control currents. One set of DFI tests specified the initial horizontal velocities to be the geostrophic velocity, calculated from the day 10 control density structure. For a second set of tests, the initial horizontal velocity was zero. The DFI was performed with four different integration times (T = 6, 9, 12, and 15 hours), and up to three repeated initialization passes for each integration time.

2. Control Simulation

The linear Rossby wave simulation resulted in the distribution of divergence, vorticity and ageostrophic currents shown in Figure 2. In the upper ocean, the maximum upward vertical velocity is co-located on the maximum divergence, and the maximum downward velocity is co-located on the maximum convergence (Figure 2.a, and 3.a). The vector form of the ageostrophic currents illustrates this convergence and divergence (Figure 2.c). A regular distribution was also found for the u and v velocities, with a slight deformation near the north and south boundaries (Figures 3.b, and 3.c). The tilted vertical structure of w, produced by the disturbance, is seen in Figure 4. The tilt of the w and v (not shown) vertical structures in the direction of the mean flow suggest a possible dampening of the fields (Pedlosky 1964).

The secondary circulation associated with the Rossby wave disturbance is in quasi-geostrophic balance. There is horizontal convergence, and horizontal divergence. The horizontal convergence has an associated pattern of downwelling that is downstream of the ridges, while the horizontal divergence has its associated upwelling pattern located downstream of the troughs. The focus of this paper is on the divergent part of the secondary circulation and its associated vertical velocity. These represent a large part of the ageostrophic current signal, and are an important part of ocean dynamics.

3. DFI Verification

As described above, the DFI method was used to try to diagnose the currents at day 10 from the control run. This is done by only using the (control) density field at that time. The accuracy of the DFI solution, as a function of the different integration time spans, was first examined by way of a normalized root mean square (rms) error (NRE). This

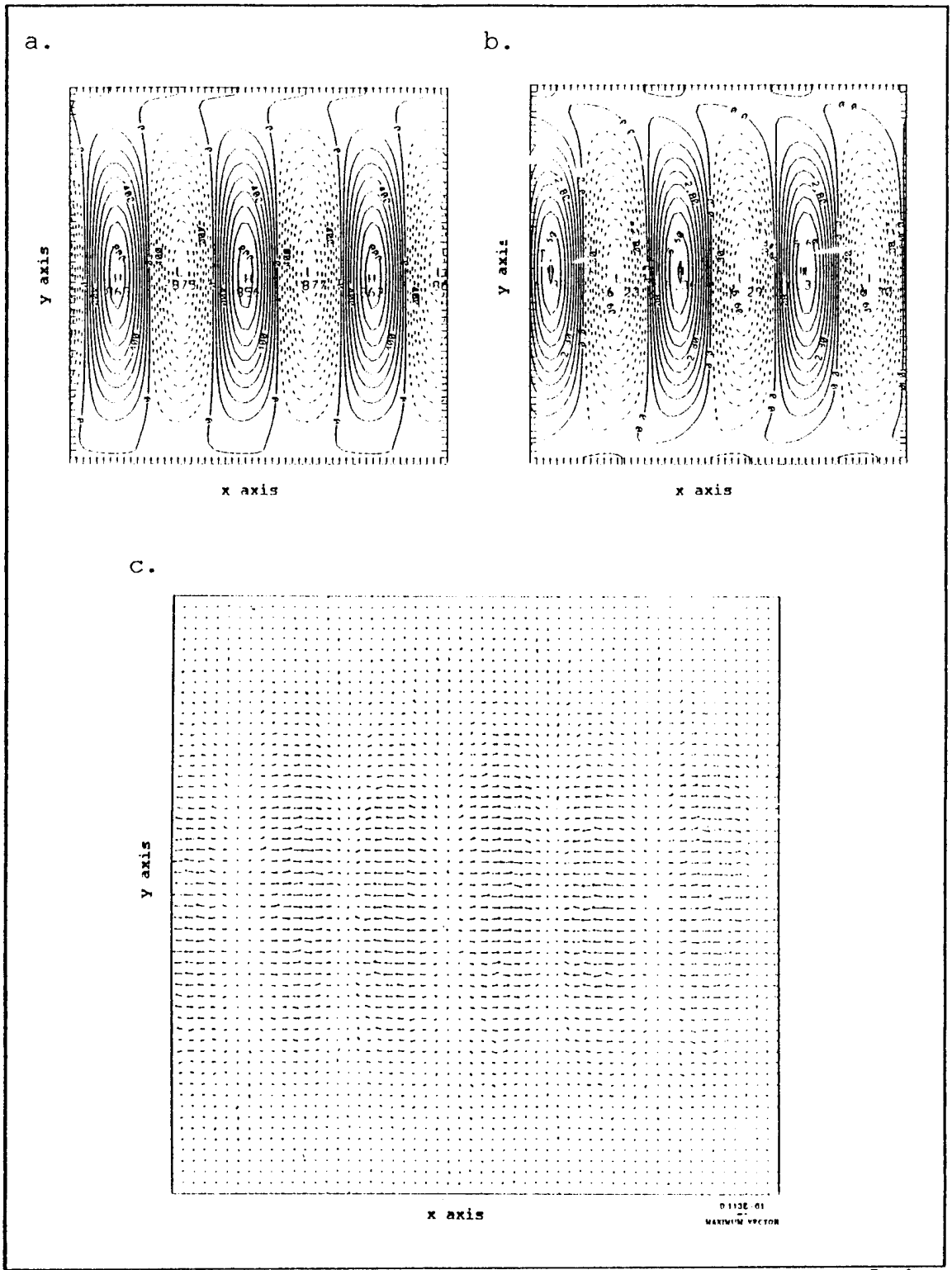

Figure 2. Rossby Wave. (a) Divergence(contour 0.01)($10^{-7}s^{-1}$). (b) Vorticity(contour 0.7)(10^{-7}). (c) Ageostrophic vector field. Negative values are dashed. Depth 65 m.

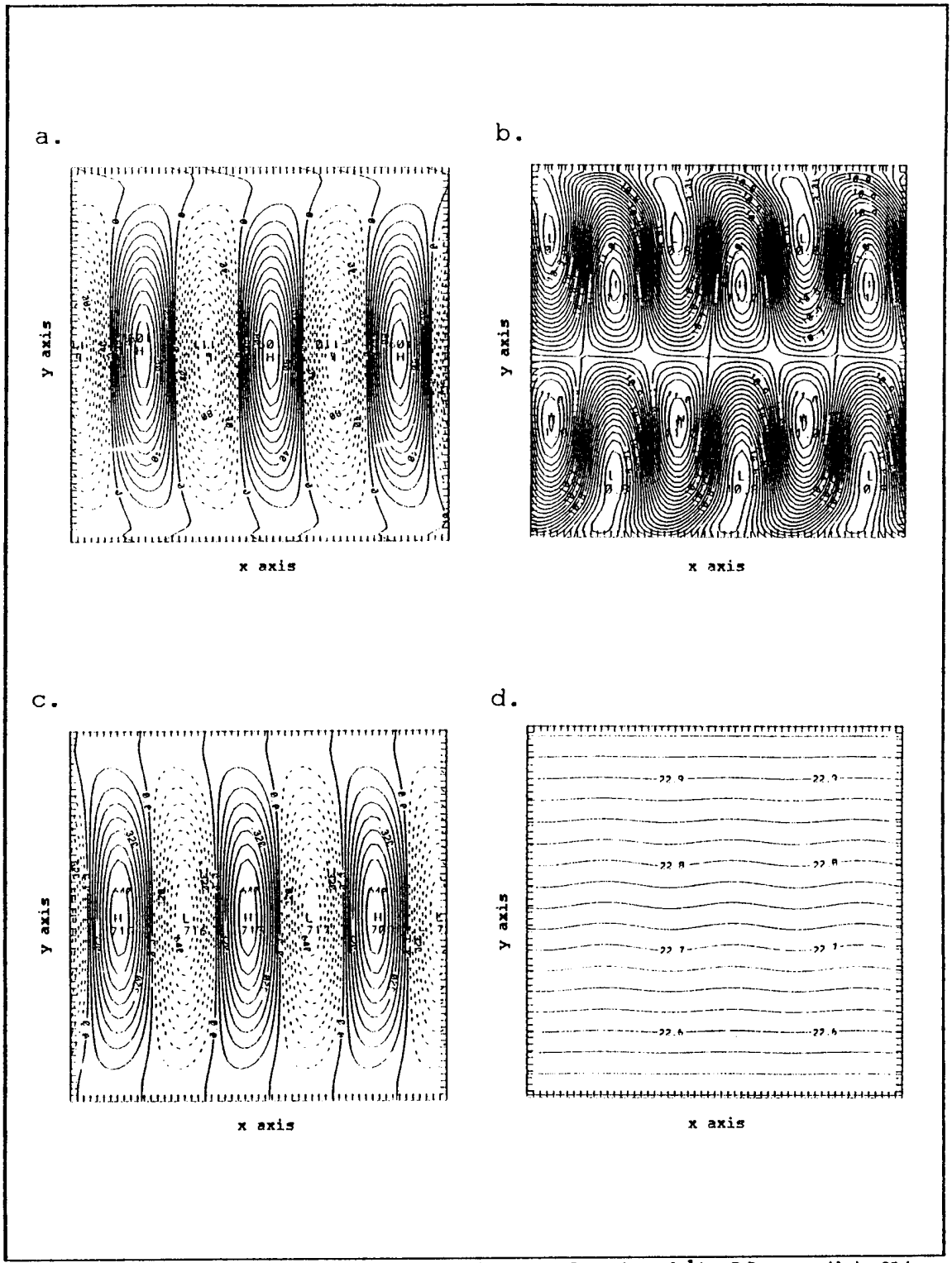

Figure 3. Rossby Wave. (a) Horizontal W(m d^{-1}),90 m. (b) U(cm s^{-1}). (c) V(cm s^{-1}). (d) Density,i.e.sigma-t(kg m^{-3}). Depth 65m for b, c,and d. Negative values are dashed.

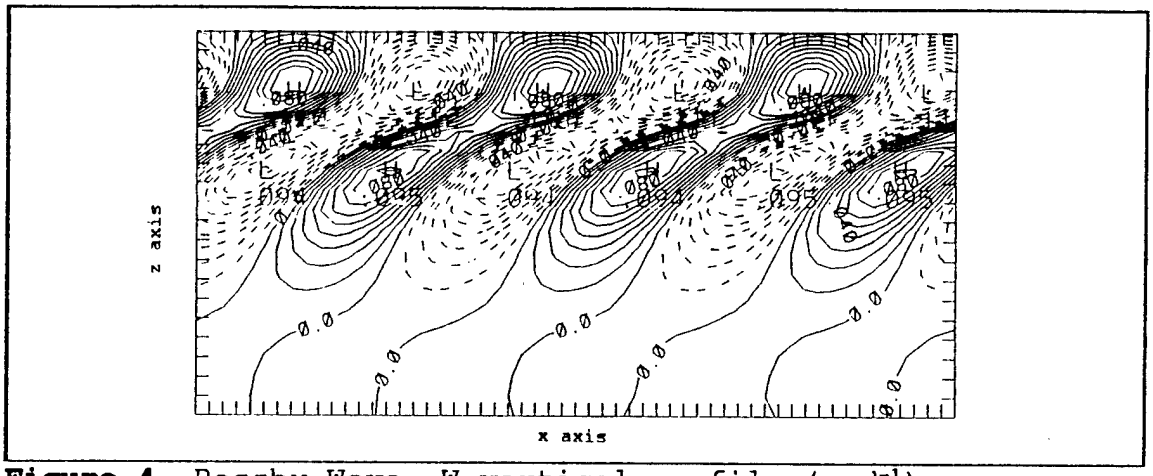

Figure 4. Rossby Wave. W vertical profile (m d^{-1}).

consisted of the rms of the difference between the vertical velocity computed from the initialized (DFI) currents, and the true (control at day 10) vertical velocity, which is then normalized by the rms of the control's vertical velocity. A percentage of the error with regard to the true vertical velocity signal is returned from Equation (3).

$$(NRE)^2 = \sum \left[\frac{(w_f - w)^2}{w^2} \right] \qquad (3)$$

In this equation the w_f represents the filtered (DFI) vertical velocity, w is the control's vertical velocity, and the summation indicates a horizontal average. In calculating the average, the outer 5 grid points in the x and y directions were not used. This eliminates from the verification any problems that might occur on the boundaries of the model due to the existence of any 'non-slow mode' behavior (gravity waves) located there.

A verification was first made for each of the four integration times (T = 6, 9, 12, and 15 hrs), with just one DFI pass. For all integration times, the control's u and v velocity fields were almost completely recovered (small NRE)

by the first DFI pass. However, the w field required the integration time to be lengthened, from T = 6 to T = 15 hrs, in order for more of it to be returned (Figure 5).

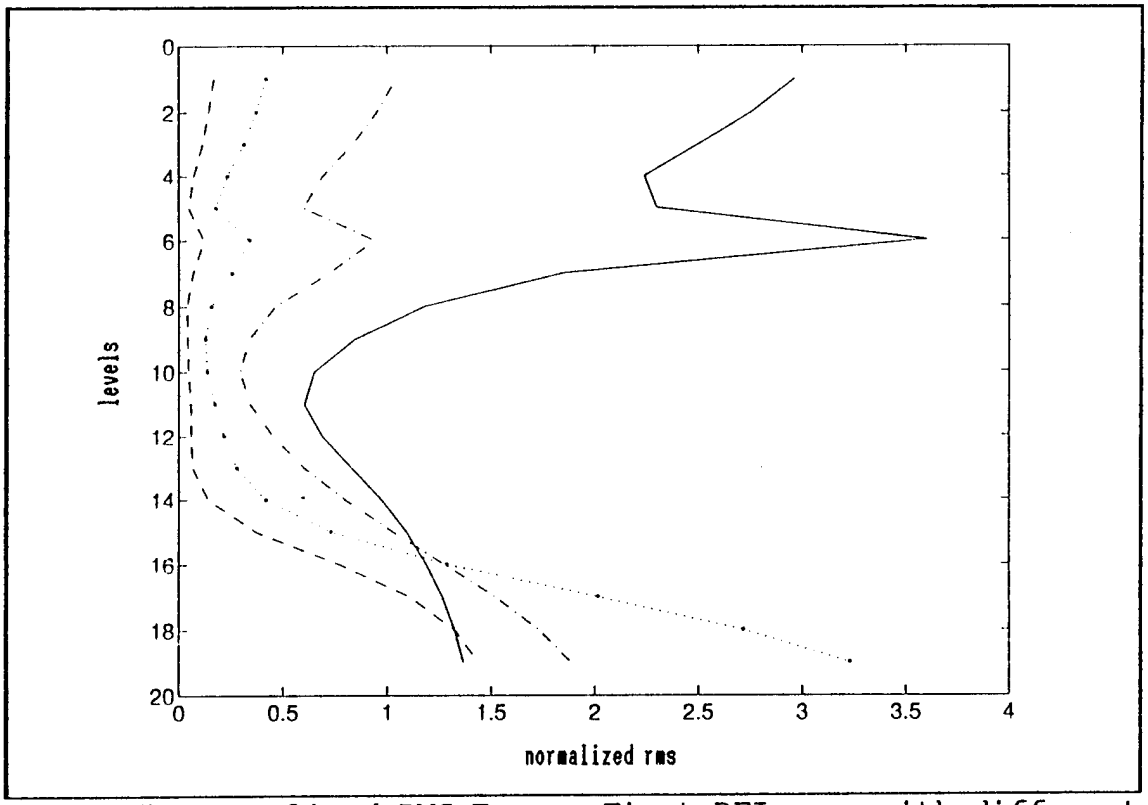

Figure 5. Normalized RMS Error. First DFI pass with different integration times. Solid line, 6-hr; dot dash line, 9-hr; dot line, 12-hr; dash line, 15-hr.

As shown in Figure 5, there is a dramatic decrease in the normalized rms error when T is increased from 6-hrs to 9-hrs. From the 9-hr to 15-hr integrations there are progressively smaller steps in advancing the accuracy. The non-convergence (NRE ~ 1) in the deeper levels is addressed below.

The results from repeating the DFI procedure (repeated "initialization") up to three times, were then compared for each integration time. For the four different integration

times (T = 6, 9, 12, and 15 hrs), the results show that the normalized rms error between the w's, decreased with the number of DFI passes (Figures 6, and 7). The least improvement concerning the normalized rms error was found in the second to third pass. Notable are the second and third passes of the 12-hr and 15-hr integration times (Figure 7). This suggests that after the second DFI pass almost all of the control vertical velocity has been recovered. When comparing pass number 3 for the different time spans, the longer integration time had the smaller normalized rms error (Figure 8). The difference in the normalized rms error between T = 12-hr 3rd pass and T = 15-hr 3rd pass, was almost negligible.

The lower model levels on all four integration times, regardless of the number of DFI passes, show an increase in the normalized rms error relative to the interior of the model. This increase of error is not a result of a difference in the magnitude of the current, but rather a difference in phase. This phase error is illustrated by comparing the zero lines of the vertical velocity profile from the control run at day 10 ,to the corresponding zero lines in the 12-hr 3rd pass profile (Figure 9). A reason for this error is that the 10-day control run had a bottom friction term, while the DFI procedure did not. In order for DFI to remain adiabatic (friction cannot be used in a backward integration) the frictional component could not be allowed in its makeup. Therefore, the zero line for the 12-hr 3rd pass DFI solution is ahead of that in the 10-day control run. This hypothesis, concerning the friction term, could be tested by rerunning the 10-day forward integration without the friction term, and then compare the vertical velocities (DFI and control) at the lower model levels to see if the phase error had been eliminated. However, this is beyond the scope of this thesis, and is left to future studies.

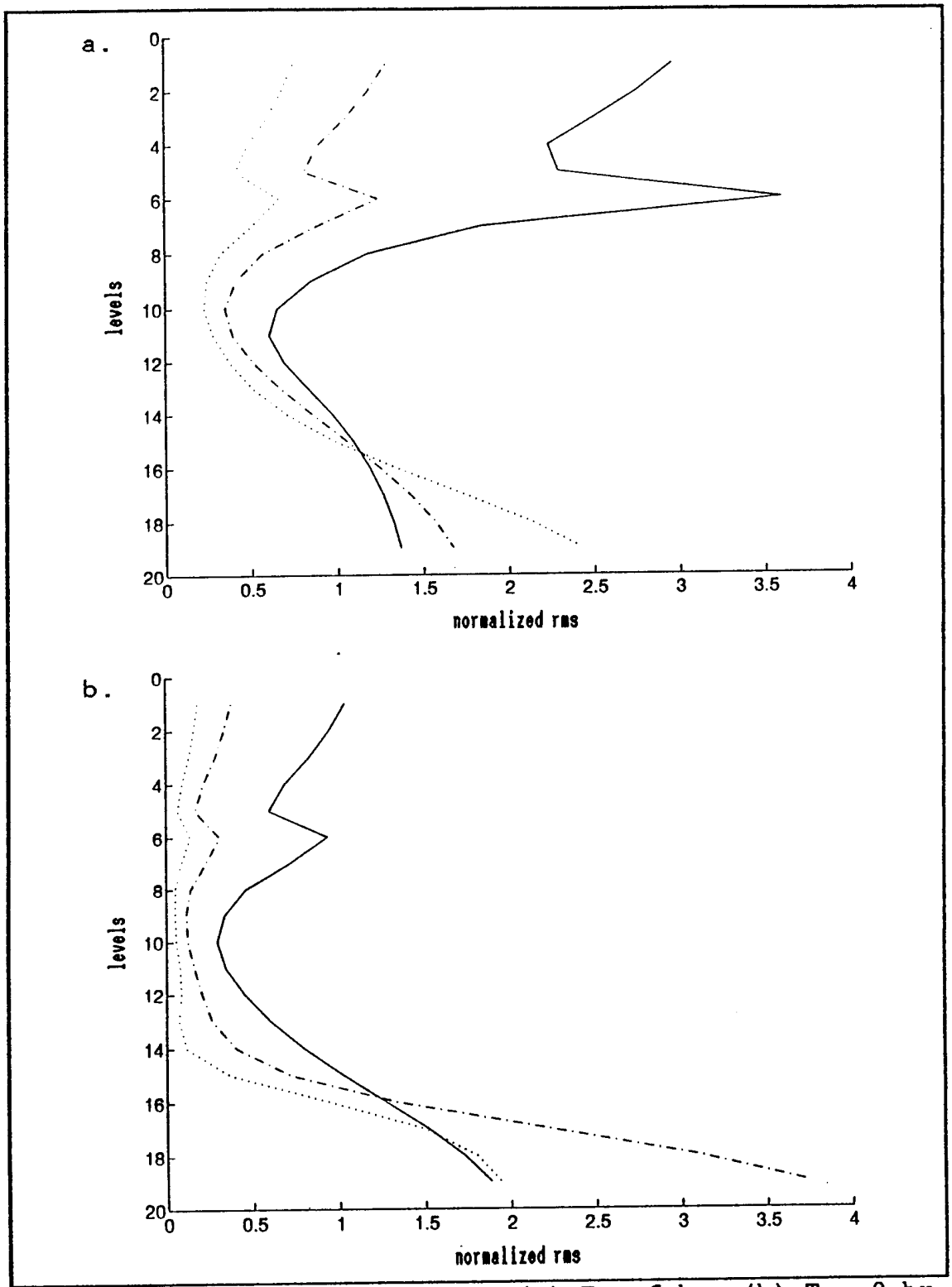

Figure 6. Normalized RMS Error. (a) T = 6-hr. (b) T = 9-hr. Solid line, 1pass; dot dash line, 2pass; dot line, 3pass.

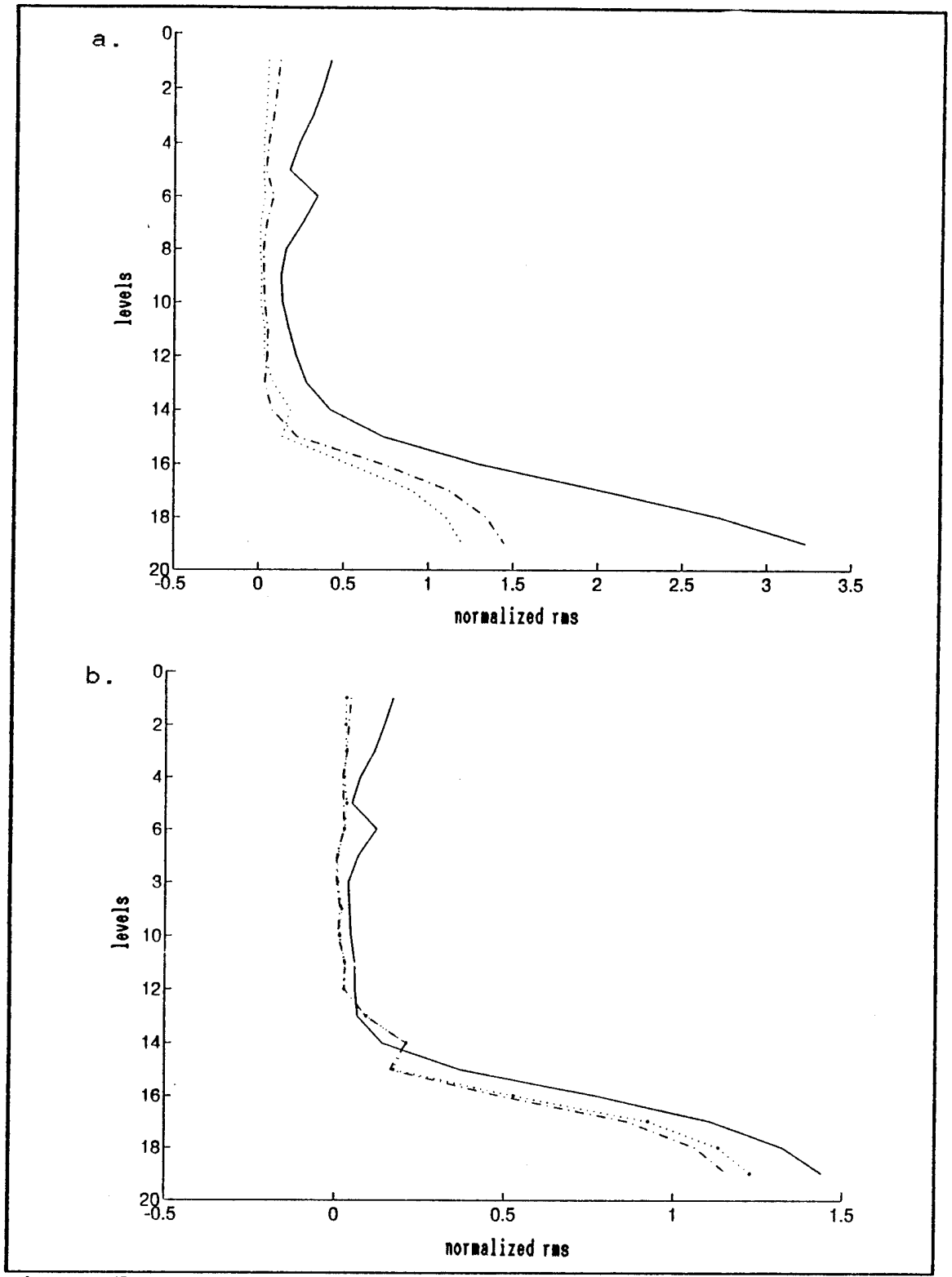

Figure 7. Normalized RMS Error. (a) T = 12-hr. (b) T = 15-hr. Solid line, 1pass; dot dash line, 2pass; dot line, 3pass.

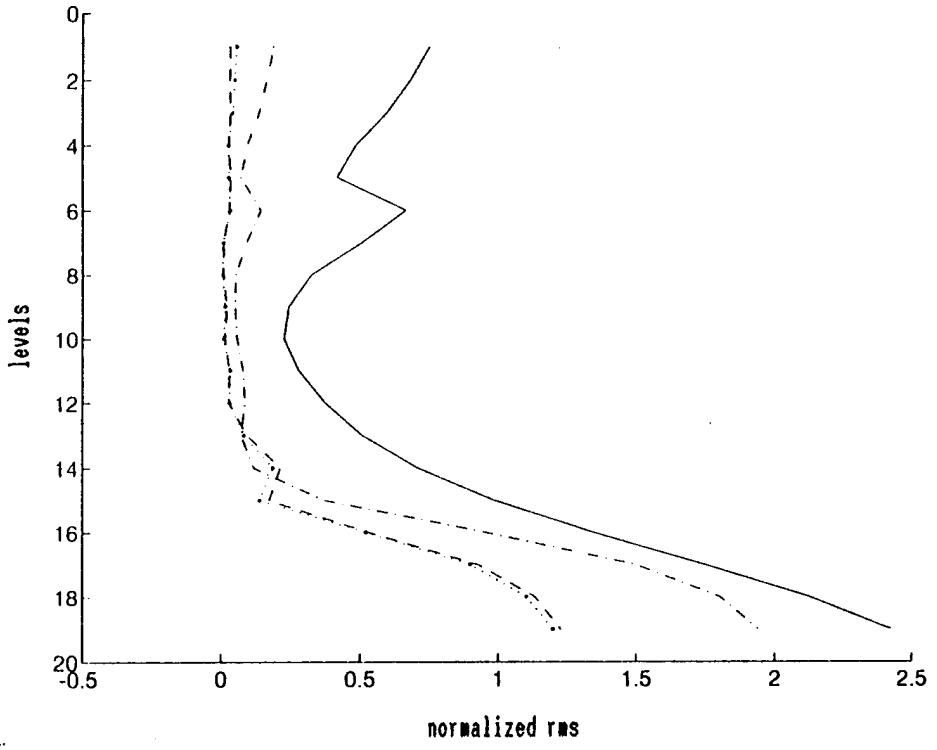

Figure 8. Normalized RMS Error. Third pass with different integration times. Solid line, 6-hr; dot dash line, 9-hr; dot line, 12-hr; dash line, 15-hr.

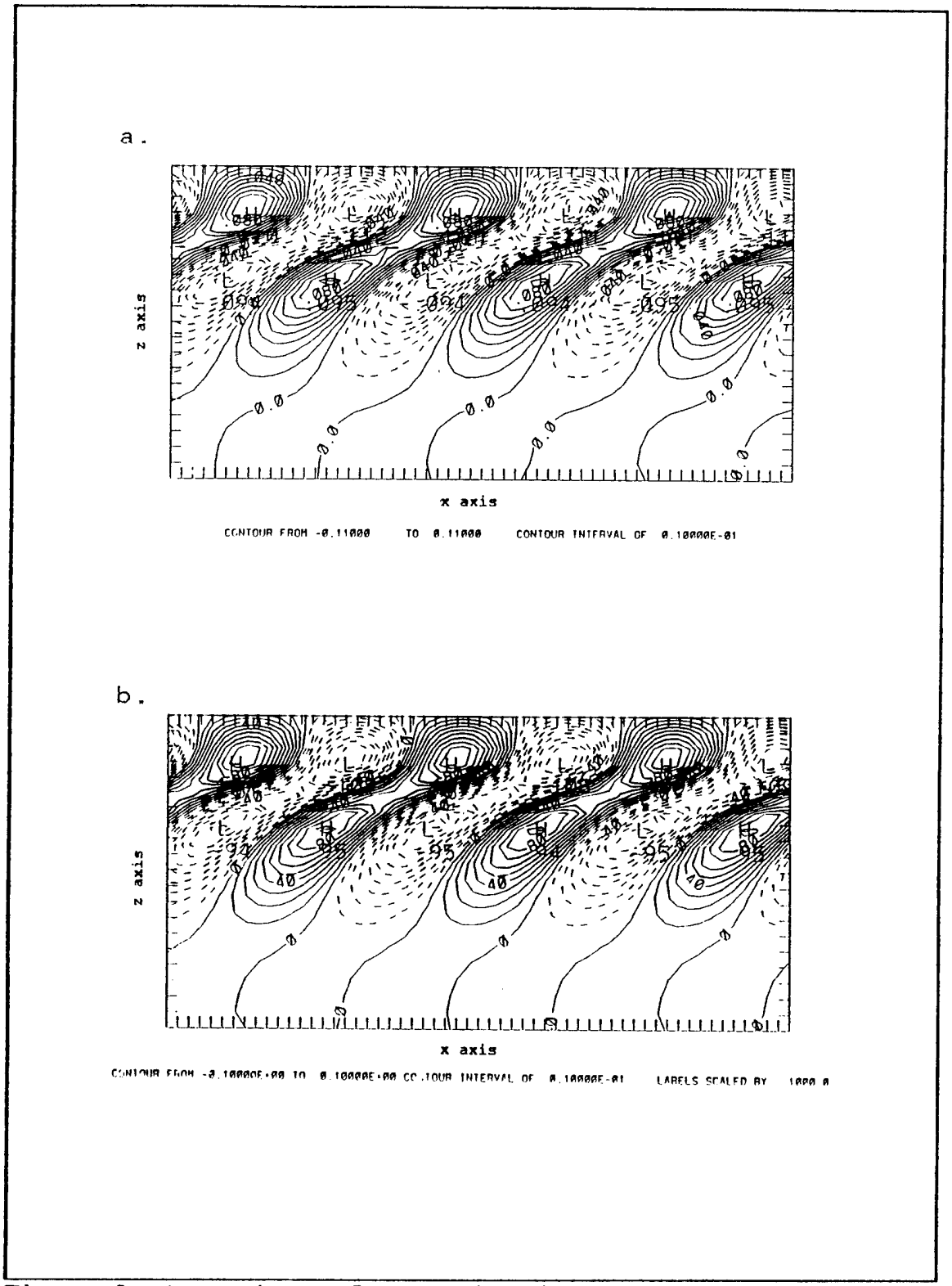

Figure 9. Comparison of Control and DFI w Vertical Profiles. (a) Control (m d^{-1}). (b) DFI, T = 12-hr 3pass (m d^{-1}).

The rms of the difference between the vertical velocities, i.e. without normalization, shows the error for the different integration times and the number of DFI passes (Figures 10, and 11). The error decreased with the number of passes and with the longer integration times. The error is large where the vertical velocity is large and it has a sharp decrease at level 5 (250 m) where there is a rapid phase change in the vertical corresponding to the bottom of the vertical exponential structure (Figure 12). This is contrasted with the normalized rms error that has a minimum value at the large vertical velocities, but a sharp increase at the vertical phase change at level 5 (Figure 13).

From the results of the different integration times and the different number of repeated DFI passes, it is clear that the 12-hr and 15-hr integration times reproduce the control the best. However, considering the increased computational time required for the 15-hr DFI integration, it does not return a normalized rms error that is significantly better than the 12-hr DFI integration. The results also show that the rms of the difference between vertical velocities is small for the 12-hr 3rd pass DFI method, at all model levels (Figure 14.a), and the normalized rms error is under 9% for all levels, except the lowest six (2250 - 4000 m)(Figure 14.b, and Table I). This increased error at the lower six levels is hypothesized to be due to the removal of the friction term in the DFI integration. The end result is that the errors are acceptably small, and that the 12-hr 3rd pass DFI method returns the original values with highly useful accuracy as shown in Figures 9, and 15.

As stated earlier, the DFI procedure was tested using two different initial velocities. The first series of tests set the horizontal velocity to the geostrophic velocities computed from the density field at the 10th day of the run. This has been reviewed above. The second series of tests set the

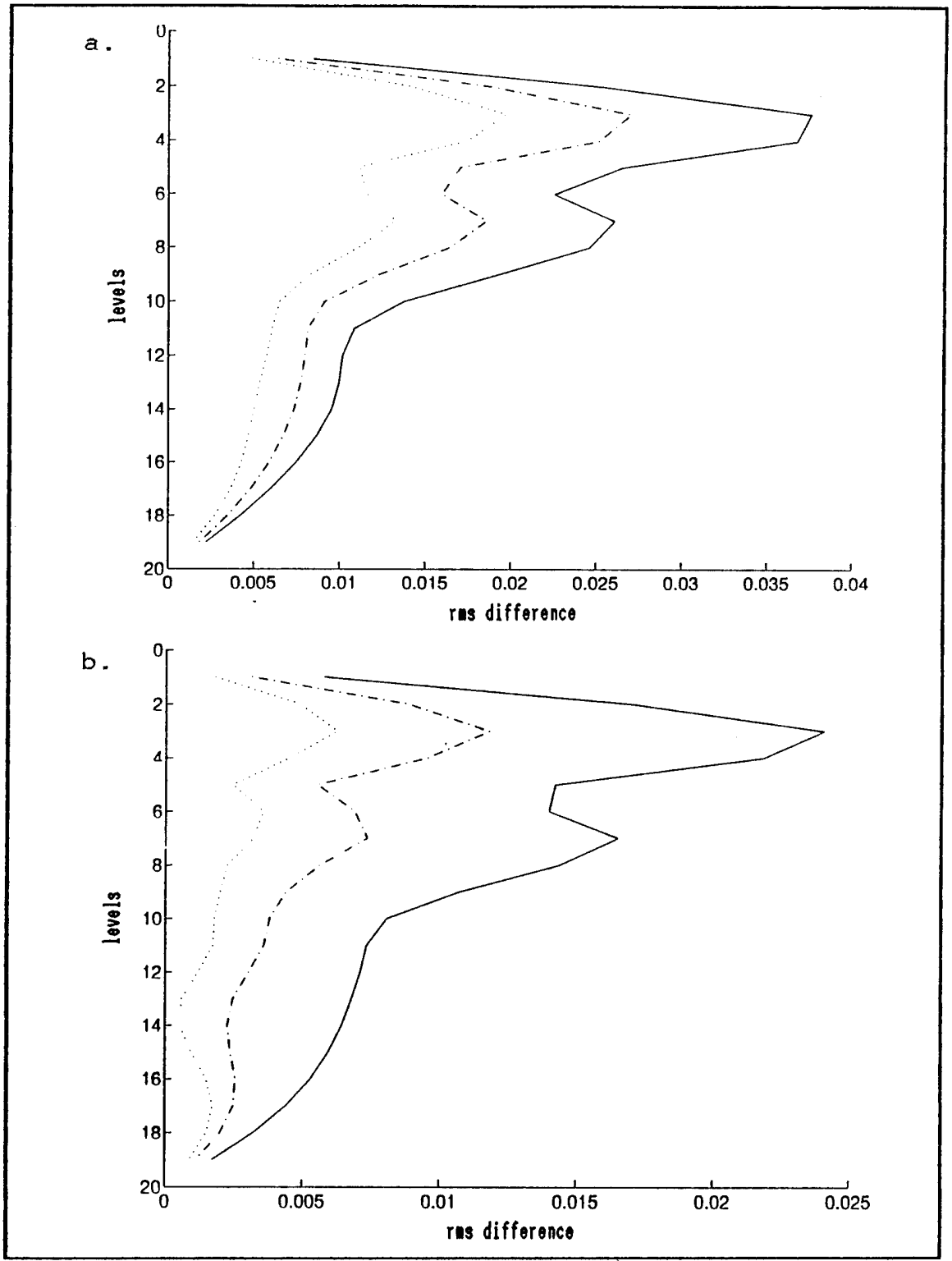

Figure 10. RMS of the Difference (m d^{-1}). (a) T = 6-hr. (b) T = 9-hr. Solid line, 1pass; dot dash line, 2pass; dot line, 3pass.

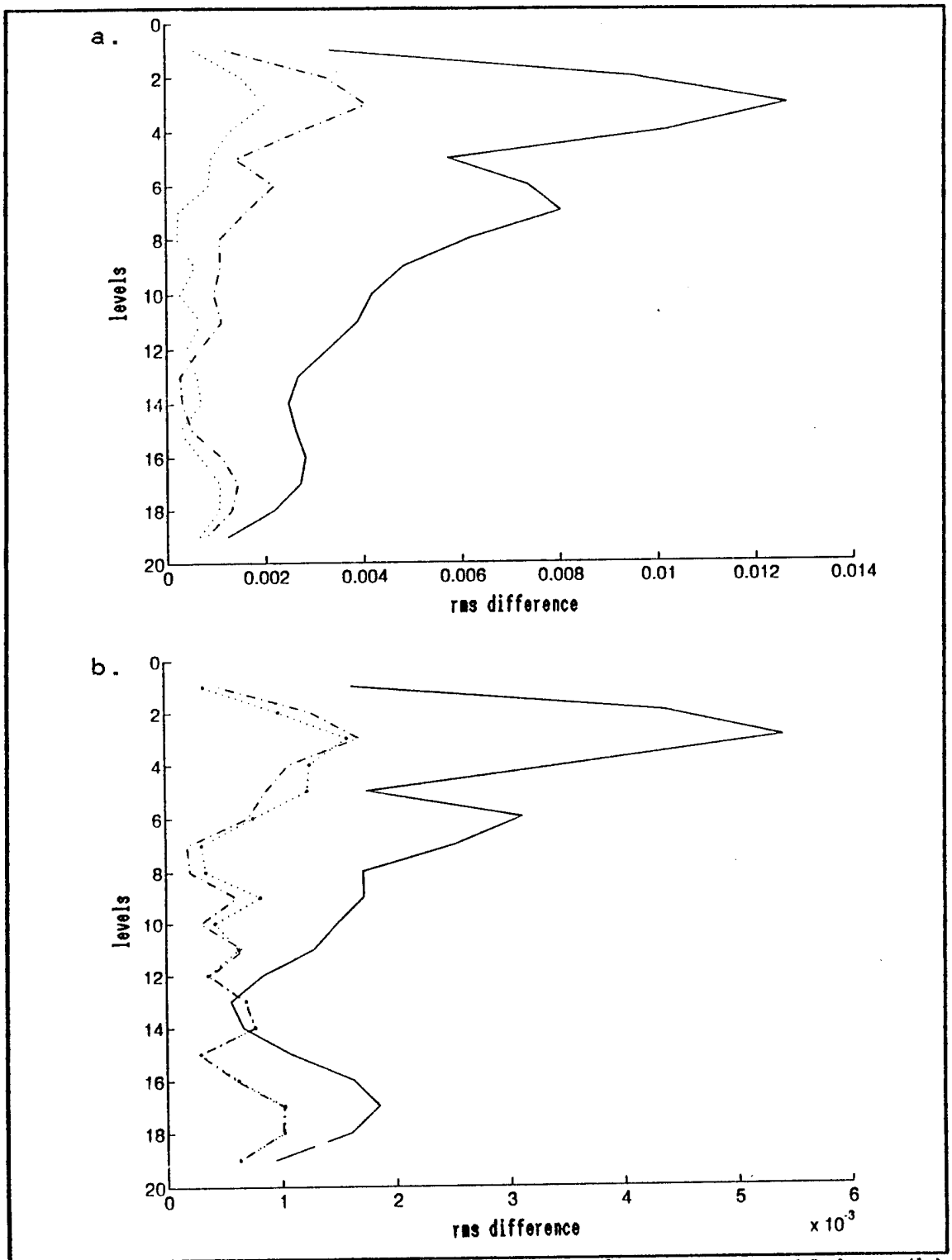

Figure 11. RMS of the Difference (m d^{-1}). (a) T = 12-hr. (b) T = 15-hr. Solid line, 1pass; dot dash line, 2pass; dot line, 3pass.

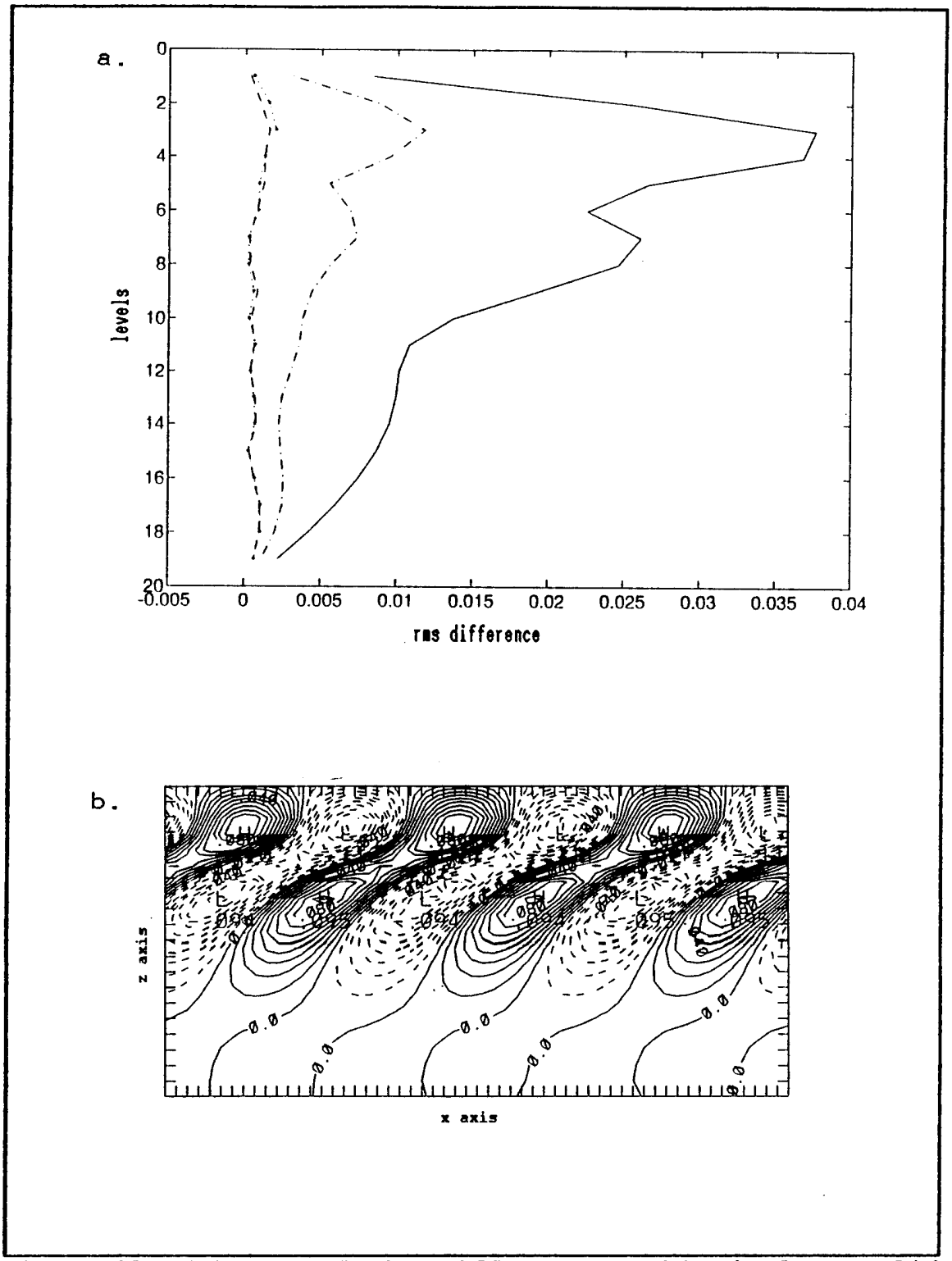

Figure 12. (a) RMS of the Difference combined plot. Solid line, 6-hr 1pass; dot dash line, 9-hr 2pass; dot line, 12-hr 3pass; dash line, 15-hr 3pass. (b) W vertical profile (m d^{-1}).

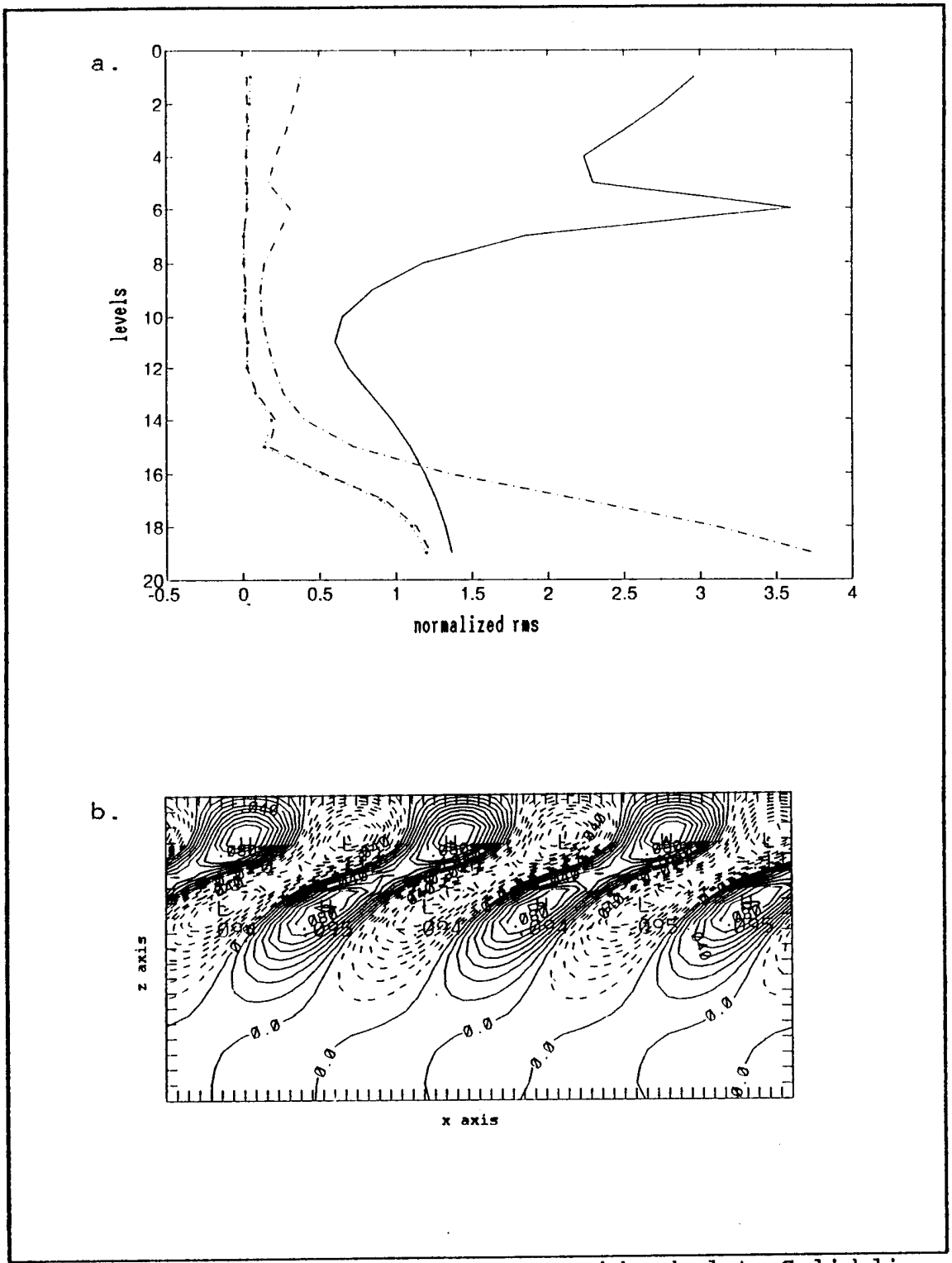

Figure 13. (a) Normalized RMS Error combined plot. Solid line, 6-hr 1pass; dot dash line, 9-hr 2pass; dot line, 12-hr 3pass; dash line, 15-hr 3pass. (b) W vertical profile (m d^{-1}).

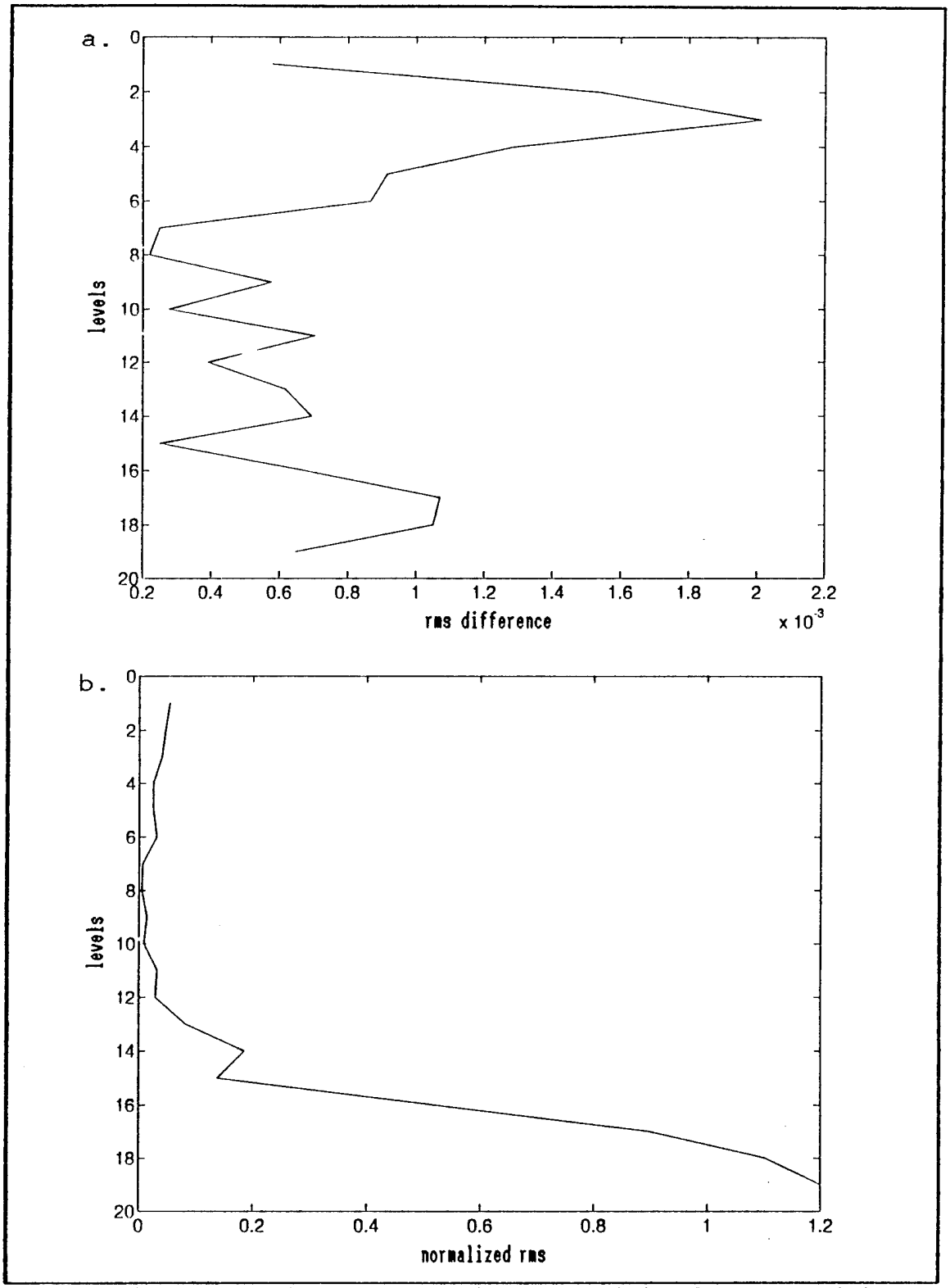

Figure 14. DFI Verification Using T = 12-hr 3passes. (a) RMS of the difference (m d^{-1}). (b) Normalized RMS Error.

Rossby Wave:

T = 12-hr 3pass

Model Level	Depth (m)	RMS DIFFERENCE RMS($w - w_t$)	NRE RMS($w - w_t$)/RMS(w)
1	10	5.7684199 E-04	5.3825520 E-02
2	40	1.5399987 E-03	4.6124276 E-02
3	90	2.0126472 E-03	3.9678775 E-02
4	160	1.2841029 E-03	2.4625398 E-02
5	250	9.1466750 E-04	2.4539951 E-02
6	360	8.6603622 E-04	3.0977732 E-02
7	490	2.4951532 E-04	6.3547445 E-03
8	640	2.1893358 E-04	4.8328936 E-03
9	810	5.7628244 E-04	1.3992130 E-02
10	1000	2.7732618 E-04	8.6974138 E-03
11	1210	7.0427696 E-04	3.2166429 E-02
12	1440	3.9193392 E-04	2.8955661 E-02
13	1690	6.1763701 E-04	8.2097113 E-02
14	1960	6.9397717 E-04	0.1856848
15	2250	2.5081812 E-04	0.1379997
16	2560	6.7364780 E-04	0.5211930
17	2890	1.0700605 E-03	0.8995180
18	3240	1.0504758 E-03	1.102790
19	3610	6.4756384 E-04	1.198437

Table I. Error Between Control and DFI w Velocities.

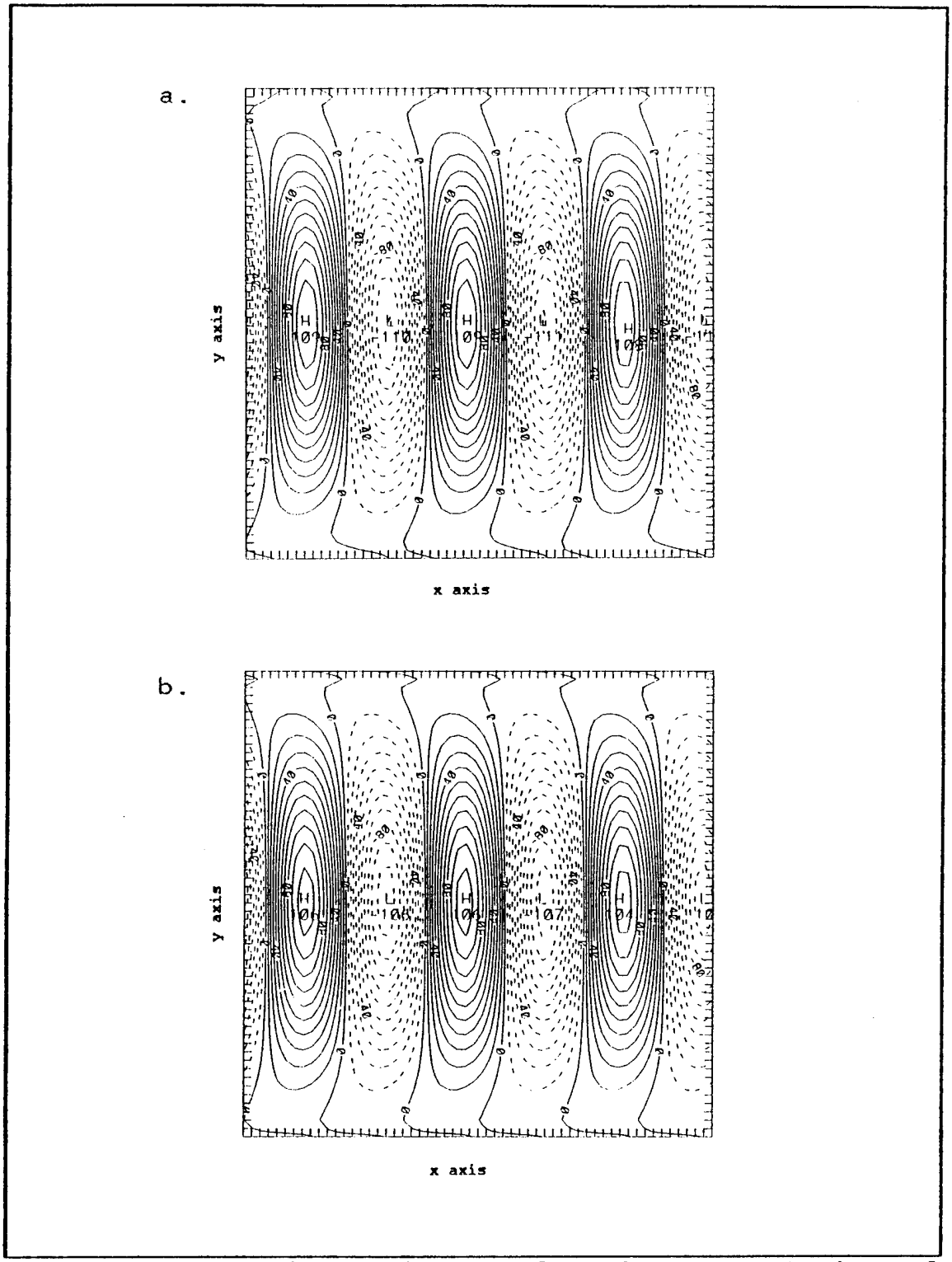

Figure 15. Comparison of Control and DFI w Horizontal Profiles, 90 m. (a) Control (m d^{-1}). (b) DFI, T = 12-hr 3pass (m d^{-1}).

initial horizontal velocities to zero, before running the DFI on the density field. This was done to examine the case of using a very poor "guess" for the initial horizontal velocities, and for theoretical curiosity. From using the geostrophic velocity as the initial velocity, it has been demonstrated above that the 12-hr time span and 3rd pass method returned the most accurate velocities. This same time span, and number of repeated passes, was used in the second DFI test in which the initial currents were set to zero.

The following equation shows the relationship between the final filtered (DFI) velocity and the geostrophic velocity determined by the initial density field:

$$V_f - V_{ig} = (V_f - V_{fg}) + (V_{fg} - V_{ig}) \qquad (4)$$

Here V_f is the filtered (dynamically balanced) velocity from DFI, and V_{ig} is the geostrophic velocity computed from the initial density field (day 10 of the 10-day integration). V_{fg} is the (filtered) geostrophic velocity computed from the initialized density field using the DFI method. The left side of Equation (4) gives the total difference (dynamical adjustment) between the final (balanced) currents and geostrophic currents determined by the initial mass field. The first pair of terms on the right hand side measure the extent to which the initialized currents are ageostrophic, while the last pair of terms measure the extent to which the density has changed during the initialization process. Which of these two pair of terms are larger will depend, obviously, on the initial currents used in the DFI procedure.

The results (not shown) indicate that the difference between the initial and final density fields (right hand side, last two terms) was larger than the difference due to the geostrophic approximation (right hand side, first two terms). This indicates that the initialized (DFI) density field was

different from the density field of the control run, and the initialized currents were in near geostrophic balance with the initialized density field. That is, the density was changed by the initialization procedure. This could be explained in terms of the scales being examined (length scale not much larger than the Rossby radius), and that the disturbance in the density field had flattened out during initialization. This flattening could be the result of no support of the density disturbance by the initial currents, which were zero. This particular result is scale dependent, and it has little practical application since geostrophic currents can (and should) always be used for the initial currents on these scales. This issue will not be investigated further in this study.

B. BAROCLINIC UNSTABLE MEAN FLOW - RUN TO FINITE AMPLITUDE

1. Setup

The baroclinic unstable mean flow was setup in the same manner as the linear Rossby wave run. The model was initialized using DFI with a 12-hr forward and backward integration that was repeated 3 times. The initial density field consisted of a disturbance superimposed on a baroclinic mean zonal jet. The disturbance was given by the following equation:

$$dist = \left[\sum_{n=1}^{N} 50 * \frac{1}{n} * \sin\left(2*\pi*\frac{n}{xm}*\left(x-\frac{xm}{2}\right)+2*\pi*rnd\right)\right] * \left[sech^2\left(\frac{(y-yd)}{y1}\right)\right] \quad (5)$$

In Equation (5), the summation extends from n = 1 to N = 14, which was the maximum zonal wavenumber used. Here xm = 112*Δx

and ym = 56*Δy, which are the x- and y- scales of the domain. This equation represents a density disturbance that is summed over 14 different wavelengths in the zonal direction. The "rnd" is a random number which will give a different phase to each wave. The longest wavelength in the x-direction is xm (n = 1), and the shortest is 8Δx (n = 14). The amplitude of each wave is inversely proportional to its wavenumber, so that the geostrophic velocity associated with that wavenumber, which is proportional to the x-derivative of the density field, will have an equal amplitude for each wavelength. The end result is a sinusoidal form of baroclinic white noise with a random phase adjustment, that contains wavenumbers from 1 to 14. This allowed the instability to select the most unstable wavenumber. The form of the density disturbance in the y-direction is the hyperbolic secant squared of ((y-yd)/y1) which has a maximum in the center of the domain and has a length scale in the y-direction of y1. This length scale y1, was set to 25 km with the result that the magnitude of the disturbance drops to 10% of the maximum in just 10 grid points (40 km). The disturbance in Equation (5) was multiplied by 50 to ensure enough initial energy was provided for the instabilities. One of the differences between this simulation and the Rossby wave simulation, is the shallower vertical profile used here. The vertical profile of the density disturbance was constant from the surface to a depth of 12.5 m, at 25 m it began a smooth transition into an exponential profile. The exponential profile had a scale depth of 100 m, which was 140 m shallower than the Rossby wave run. Another difference alluded to earlier was the model's domain was doubled in the x-direction for this test (from 56 to 112 grid points). This increase of length was to allow more room in which the different wavelengths could develop. With Δx = Δy = 4 km, the east to west distance became 448 km, while the north to south distance remain at 224 km.

The mean zonal shear flow that the density disturbance was superimposed, was produced from the same density structure (hyperbolic tangent) as in the Rossby wave run. However, the width of the current (y1) was reduced from the 1000 km used with the Rossby wave, to 25 km. This tightened the baroclinic flow from which the instabilities would grow. The vertical profile of the mean flow (i.e. the axis of the jet) was also shifted toward the south with depth, which resulted in the mean flow being centered slightly south of the center of the y-axis. The southward tilt in the zonal flow increased the instability in the model by increasing the vertical shear. The increased shear increased the instabilities in the model and helped the disturbances grow quickly. Besides the tilt, the zonal shear flow was also multiplied by the same shallow z-dependent function, as the density disturbance (constant in z above 12.5 m, at 25 m a transition to an exponential function with a 100 m scale depth).

The model was integrated forward 40 days after the DFI initialization in order to produce the control run. This was to allow the instabilities to grow and develop to a sufficient magnitude. The instantaneous density field was extracted from the 40th day, and used in the following DFI tests in an attempt to recover the control currents. The geostrophic velocities calculated from the day 40 density structure were used as initial horizontal velocities for the DFI. The DFI tests were performed with three different integration times (T = 9, 12, and 15 hours), and up to three repeated initialization passes, for each of the integration times.

2. Control Simulation

The baroclinic unstable flow simulation resulted in a sinusoidal distribution (zonal wavenumber 2) of divergence, vorticity and a tilted zonal distribution for the w velocity at day 40 as shown in Figures 16, and 17.a. The ageostrophic vector field (Figure 17.b) shows a series of cells (rotational

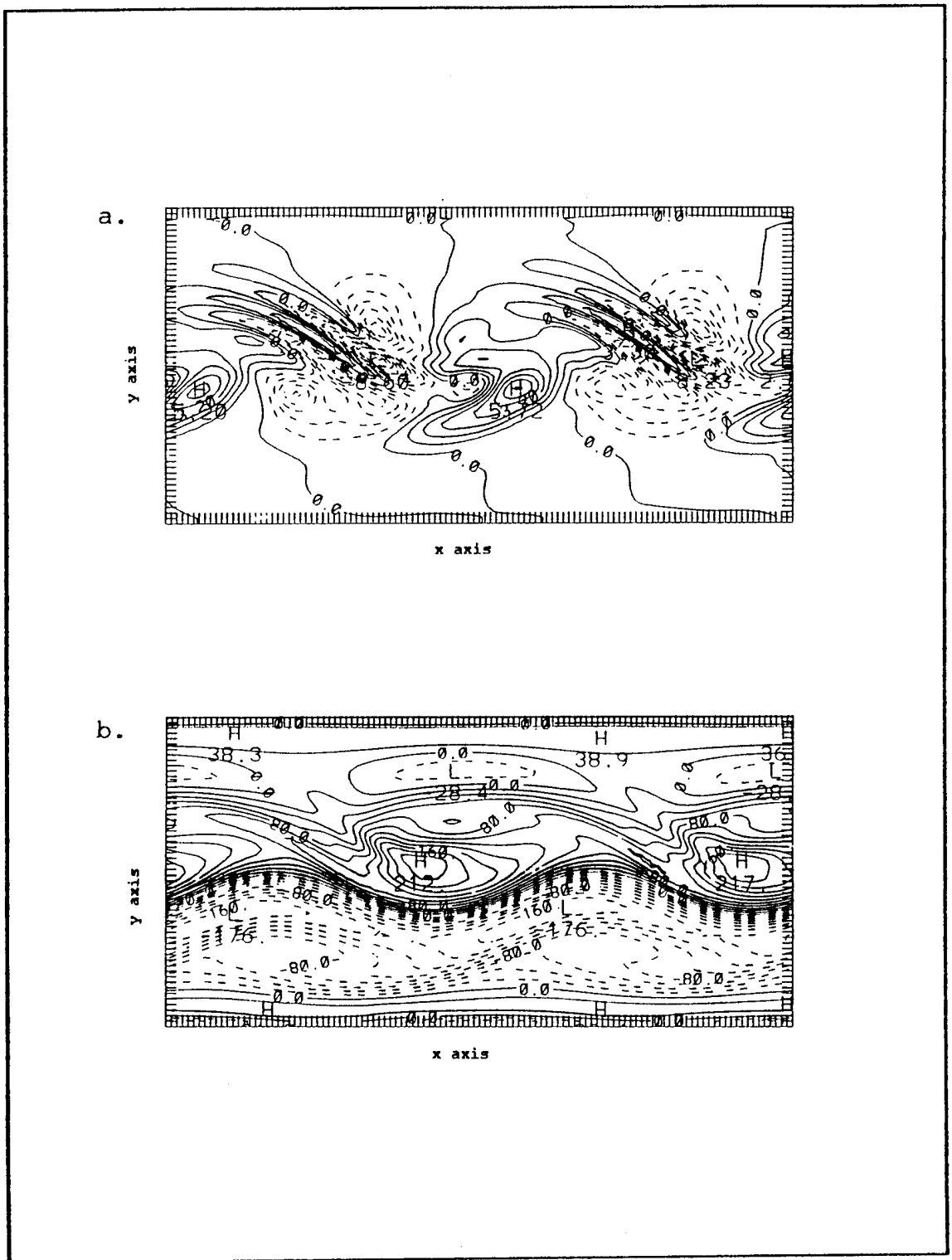

Figure 16. Unstable Baroclinic Flow. (a) Divergence(contour 0.8)($10^{-7}s^{-1}$). (b) Vorticity(contour 20.0)($10^{-7}s^{-1}$). Negative values are dashed. Depth 65 m.

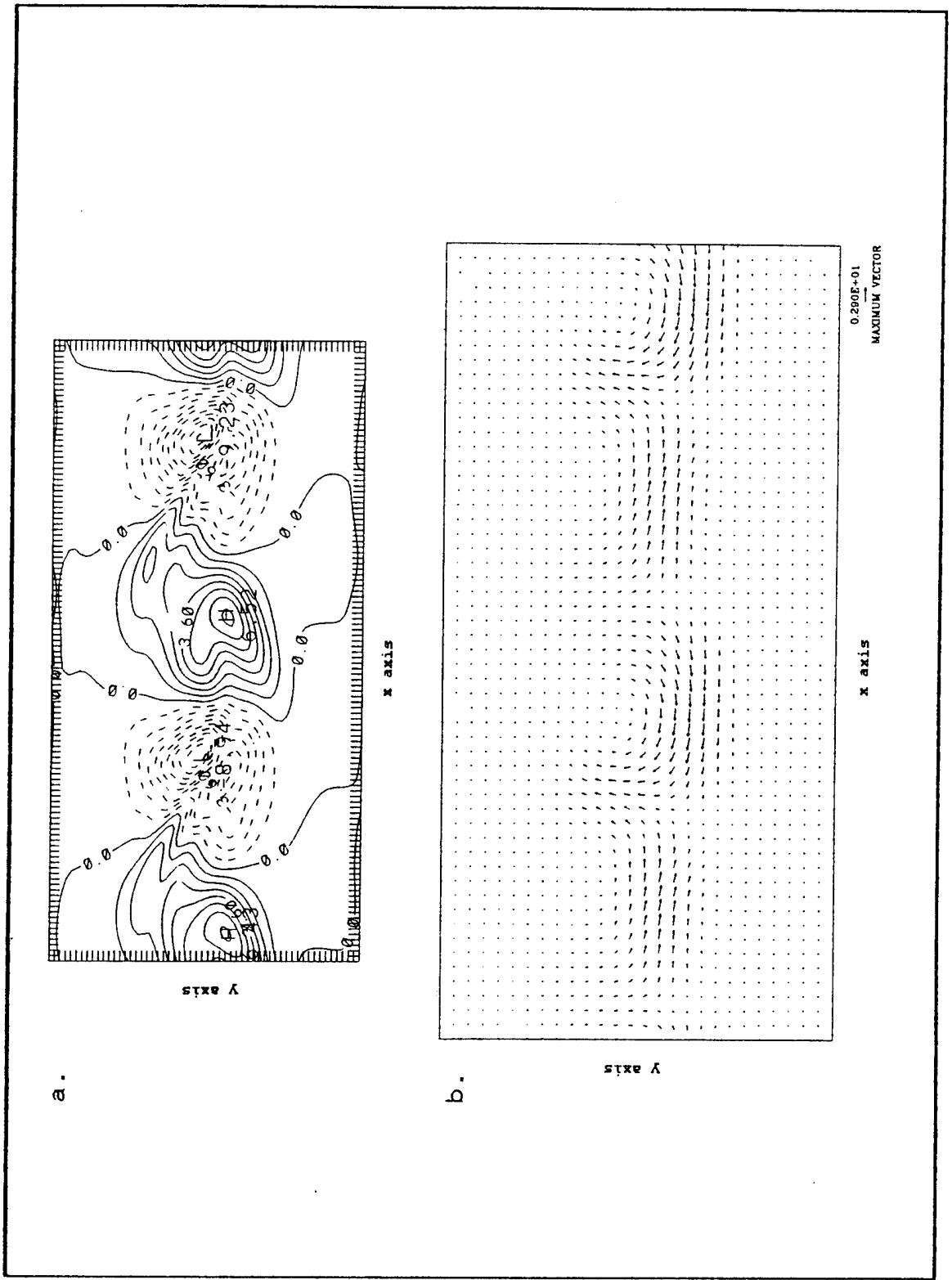

Figure 17. Unstable Baroclinic Flow. (a) W horizontal profile (m d^{-1}), 90 m. (b) Ageostrophic vector field, 65 m.

flow) which creates the areas of maximum divergence that produces the corresponding areas of maximum upward vertical velocity. The rotational flow also causes the areas of maximum convergence and their corresponding areas of maximum downward vertical velocity.

Density, w velocity, and the v velocity field all show the sinusoidal pattern with the dominant zonal wavenumber 2 (Figures 18, 19.a, and 19.b). The u velocity pattern has a split sinusoidal form with the isotachs concentrating in or just ahead of the troughs and expanding in or just ahead of the ridges in the parallel flows (Figure 19.c). The resulting w field is in quasi-geostrophic balance (v and w in phase), with rising motion ahead of the troughs and sinking motion ahead of the ridges as seen in Figures 19.a, and 19.b.

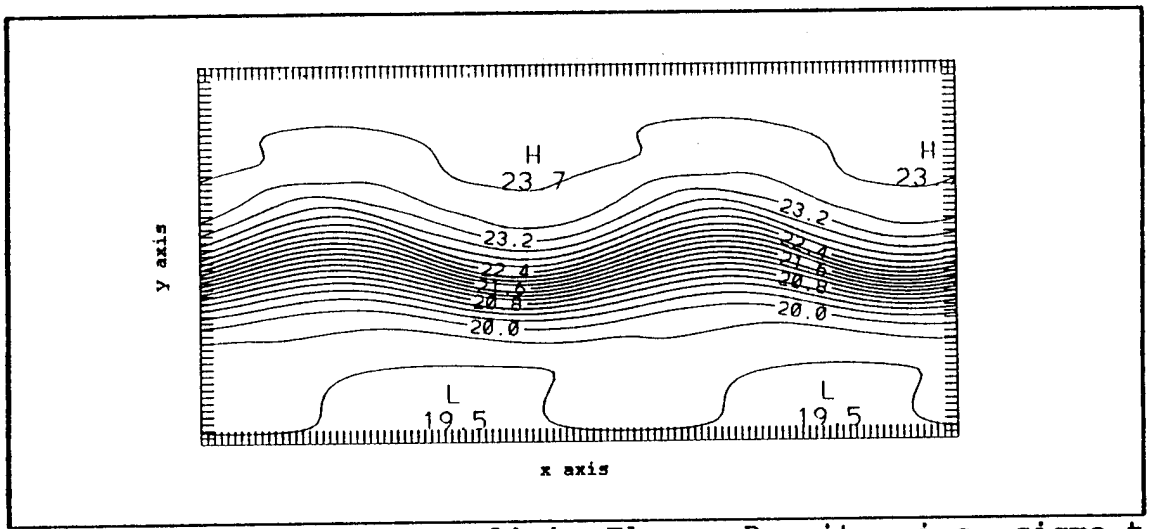

Figure 18. Unstable Baroclinic Flow. Density, i.e. sigma-t (kg m^{-3}), at 65 m.

3. DFI Verification

Similar to the Rossby wave tests, the DFI method was used here to try to recover the currents at day 40 of the control run, using only the (control) density field from that time. Utilizing the normalized rms error (Equation (3)) the accuracy of the DFI solution was examined. The DFI was examined with regard to the different time spans, and to the different

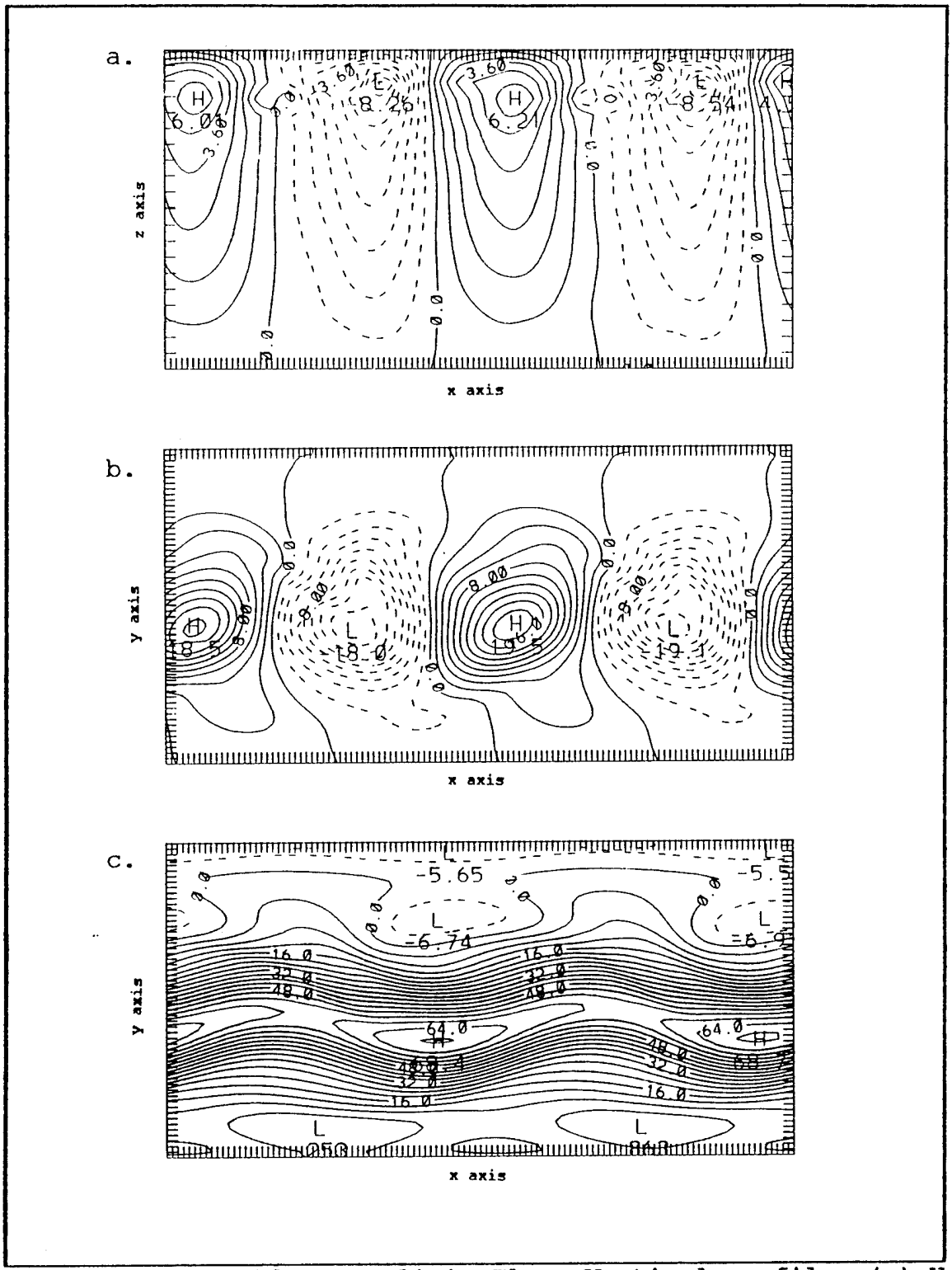

Figure 19. Unstable Baroclinic Flow. Vertical profile: (a) W (m d^{-1}). Horizontal profile: (b) V (cm s^{-1}); (c) U (cm s^{-1}). Horizontal profiles at 65 m.

number of passes of integration.

The first verification was made for just one DFI pass for each of the three integration times (T = 9, 12, and 15 hrs). For all time spans, the control's u and v velocity fields were almost completely recovered by the first DFI pass. However, the w field required the integration time to be lengthened, from T = 9 to T = 15 hrs, in order for more of it to be returned (Figure 20). As shown in Figure 20, there is a dramatic decrease in the normalized rms error when T is increased from 9-hr to 12-hr. There is a smaller increase in accuracy between the 12-hr and 15-hr integration. As in the Rossby wave case, the error remains significant (NRE ~ 0.4) near the bottom. However, in this case it is also higher near the surface. The interpretation of this error is given below.

The DFI procedure was then repeated up to three times, and the results were compared for each integration time. These results show that for the three different integration times (T = 9, 12, and 15 hrs), the normalized rms error between the w's, decreased with the number of DFI passes (Figures 21 and 22). The least improvement with regard to the normalized rms error was found in the second and third passes. Notable are the second and third passes of the 15-hr integration (Figure 22). This indicate that after the second DFI pass almost all of the control vertical velocity has been recovered. Figure 23 shows that for the different time spans at the 3rd pass, the longer integration times had the smaller normalized rms error. The difference between T = 12-hr 3rd pass and T = 15-hr 3rd pass with regard to the normalized rms error was insignificant.

The lower model levels, for all four integration times, show an increase in the magnitude of the normalized rms error. This increase of error is due to a combination of effects. First, there is a slight phase error in the vertical velocities. By comparing the zero lines of the control and

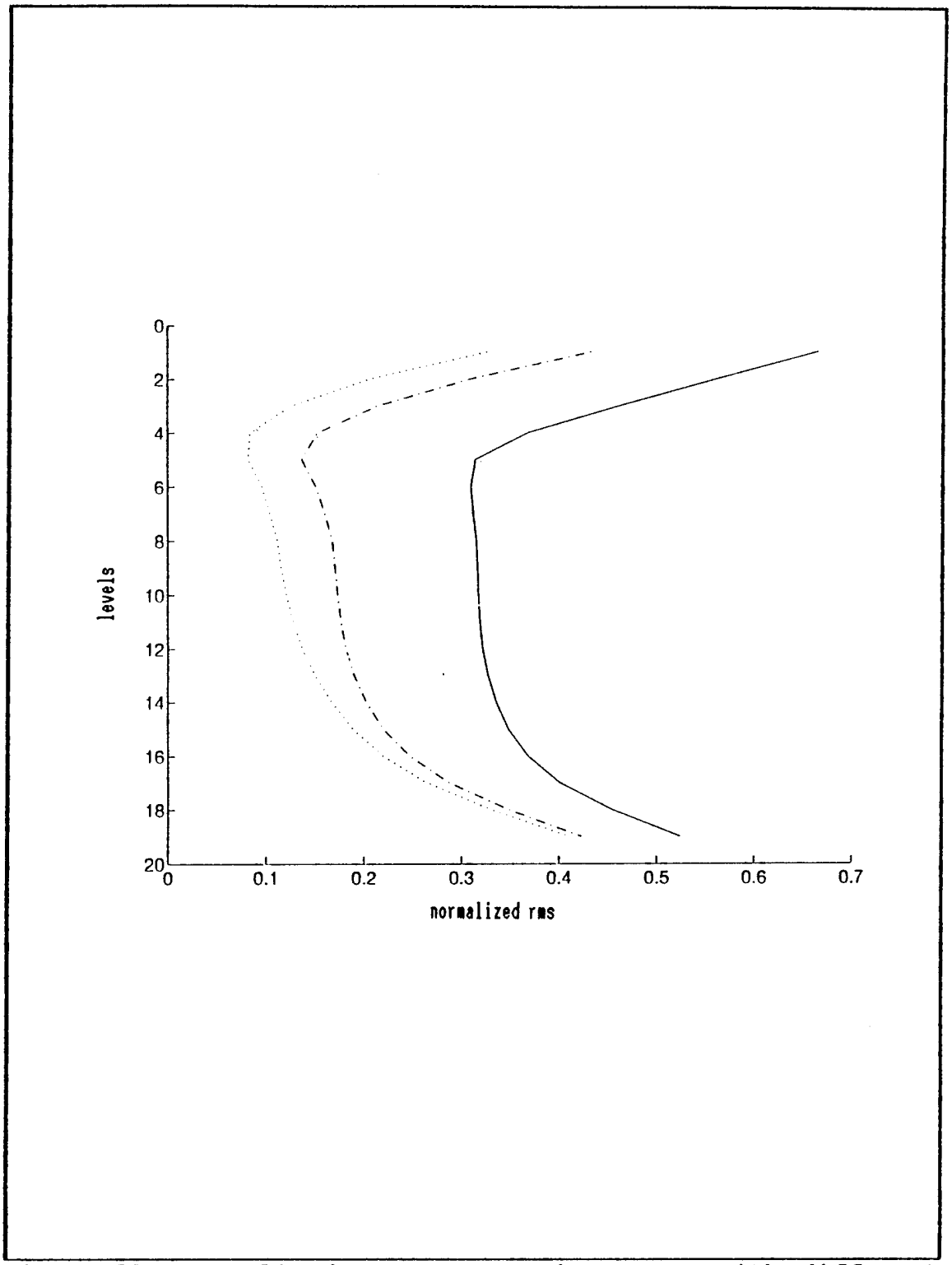

Figure 20. Normalized RMS Error. First pass with different integration times. Solid line, 9-hr; dot dash line, 12-hr; dot line, 15-hr.

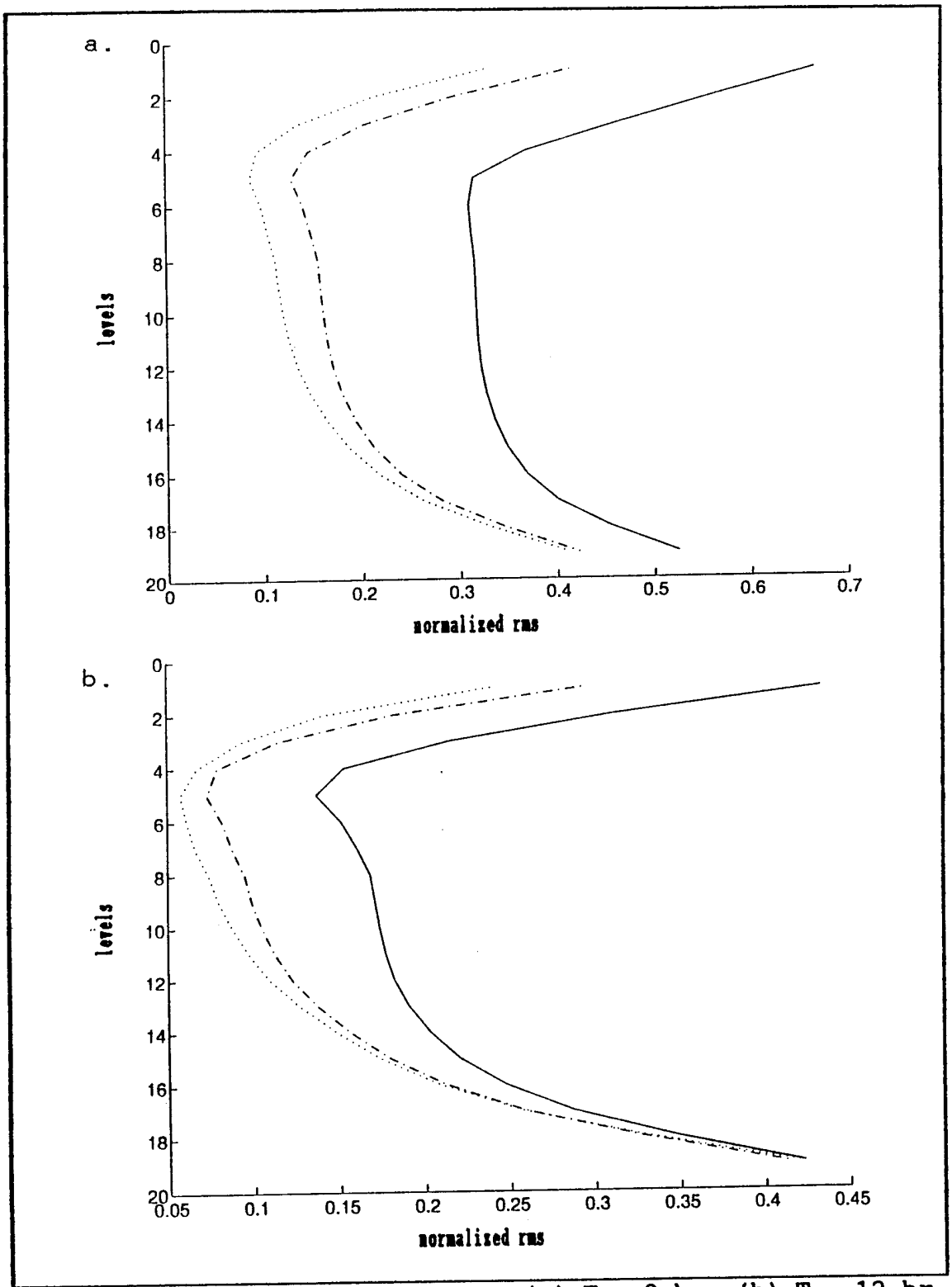

Figure 21. Normalized RMS Error. (a) T = 9-hr. (b) T = 12-hr. Solid line, 1pass; dot dash line, 2pass; dot line, 3pass.

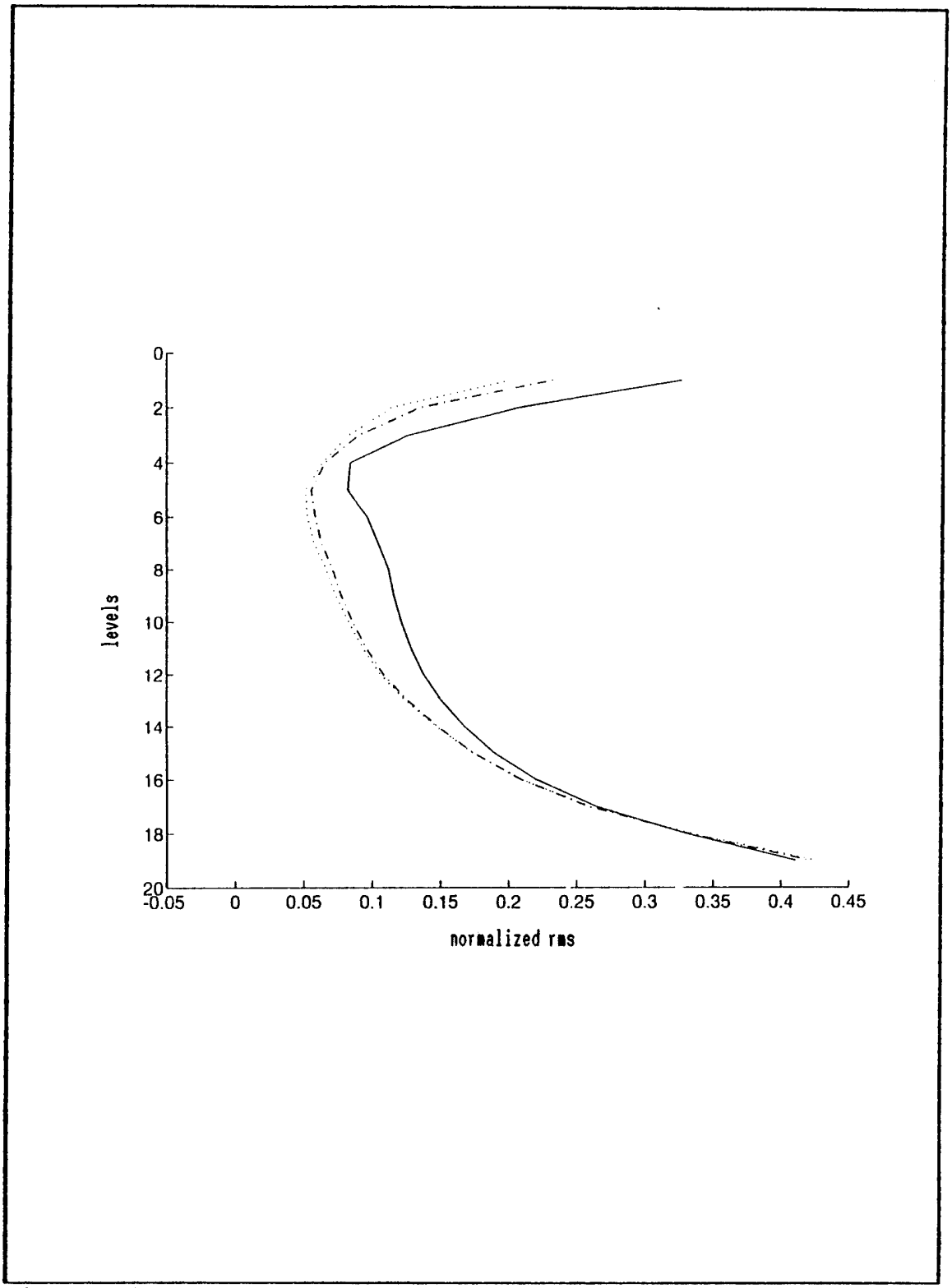

Figure 22. Normalized RMS Error. (a) T = 15-hr. Solid line, 1pass; dot dash line, 2pass; dot line, 3pass.

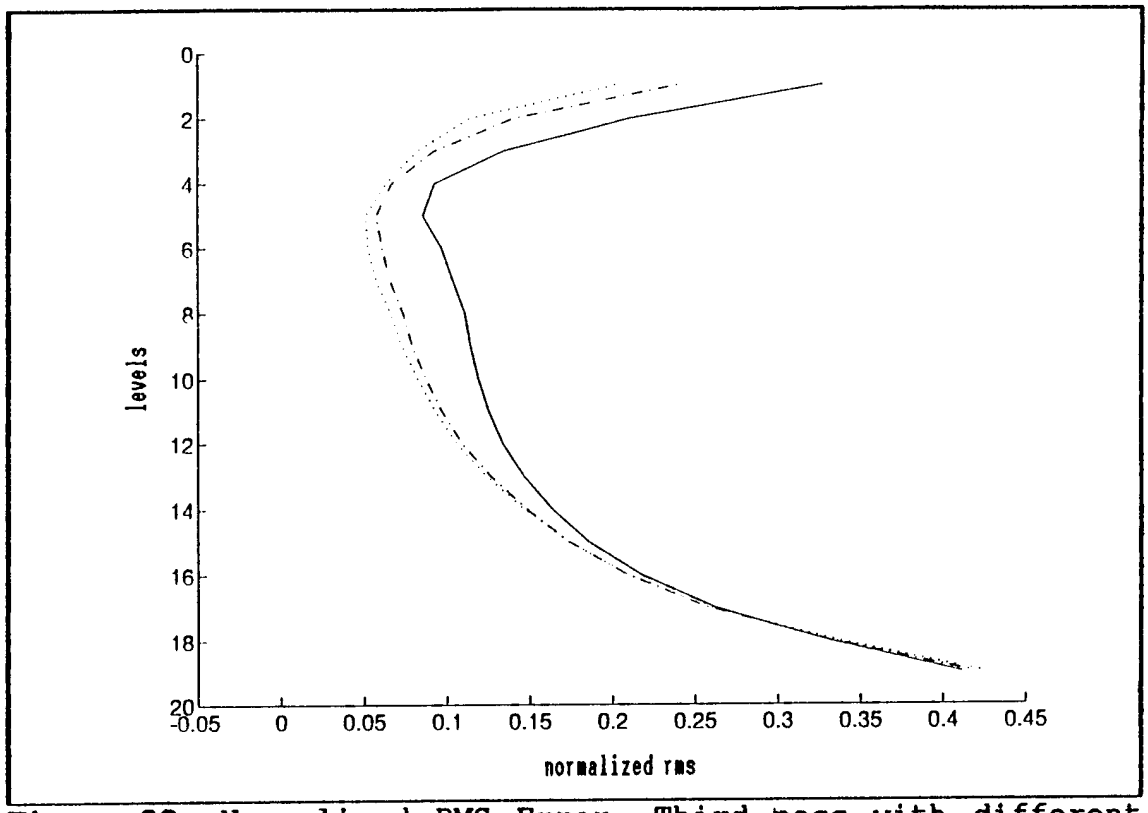

Figure 23. Normalized RMS Error. Third pass with different integration times. Solid line, 9-hr; dot dash line, 12-hr; dot line, 15-hr.

DFI vertical velocity, in Figure 24, it is seen that near the western edge of the domain the DFI zero line is slightly ahead of the control, but in the middle of the domain they are the same, then the control moves ahead of the DFI at the eastern edge. One would have thought because the 40-day control run had a bottom friction term, while the DFI procedure did not, that the DFI zero line would consistently be ahead of the control's zero line as in the Rossby wave case. Instead, only part of the normalized rms error is due to a phase error.

The second part of this normalized rms error can be found by looking again at Figure 24. There it is seen that the DFI run has positive contours going slightly deeper than the contours for the control at the lower levels. The negative contours also extend deeper. This would indicate a slight

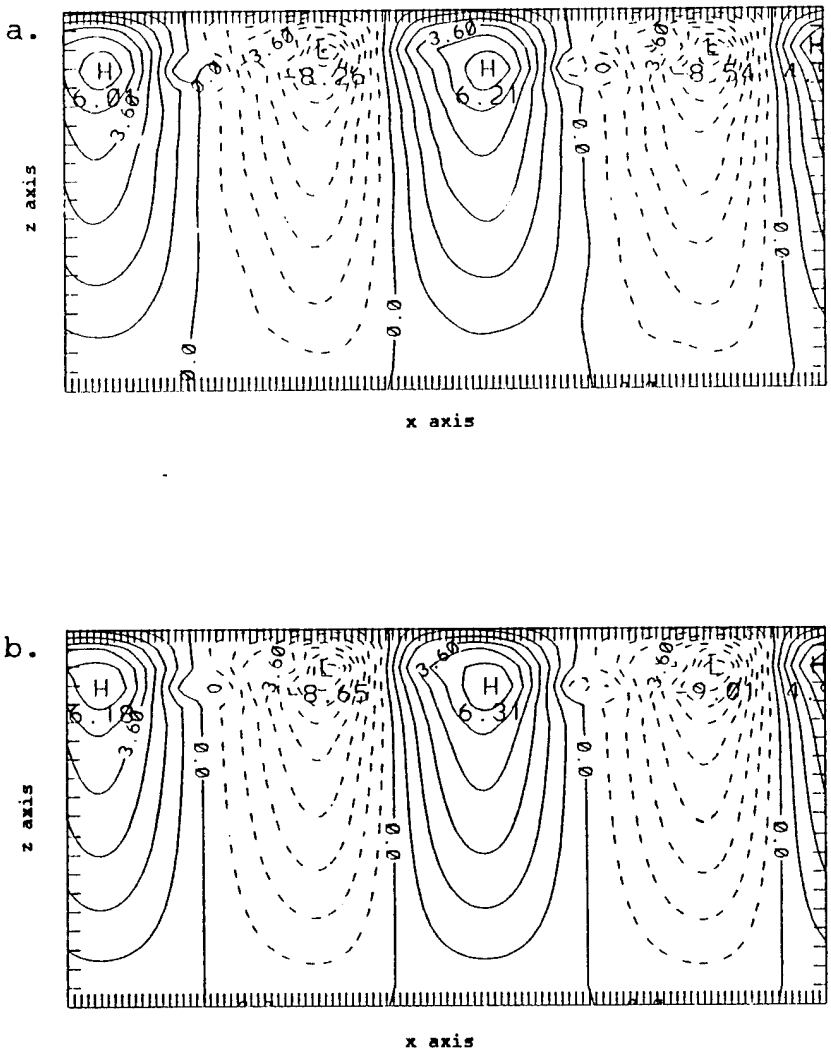

Figure 24. Comparison of Control and DFI w Vertical Profiles. (a) Control (m d^{-1}). (b) DFI, T = 12-hr 3pass (m d^{-1}).

magnitude error in the recovery of the currents at these depths with the DFI solution somewhat stronger. This is also seen by the larger central values (amplitudes) for the DFI solution. A rapid increase in the percent of error is also observed near the surface. It appears here too, that the positive contours for the DFI are just a bit larger than the control's. These larger errors, that occur in both the shallower and deeper parts of the domain, are located where the model's resolution of the phenomenon is poorest. For the error near the surface, there is a shallow vertical scale that only extends over 1 or 2 model levels. In the deeper ocean, the vertical levels are grouped farther and farther apart. This hypothesis could be addressed by increasing the vertical resolution. The simulation could be done again with the results compared between the control and DFI to see if the normalized rms error had decreased. This was not done and left for future study. Another possible explanation is the fact that the DFI solution is adiabatic (no friction), so the amplitude of the disturbances are not damped as in the control run. Comparing the central values of Figures 24 show the larger magnitudes of the DFI currents. The actual test of this premise would require a frictionless control run, which was also left for a future study.

Though the normalized rms error increased at the surface and at the lower 7 levels, the absolute error at these locations is small for all time spans. The rms of the difference between the vertical velocities (i.e. not normalized), shows the absolute error for the different integration times and the different number of DFI passes (Figures 25, and 26). The absolute error decreased with the number of passes and with the longer integration times. The absolute error is large where the vertical velocity is large at level 3 (90 m)(Figure 27). This behavior is contrasted with that of the normalize rms error that has a minimum value

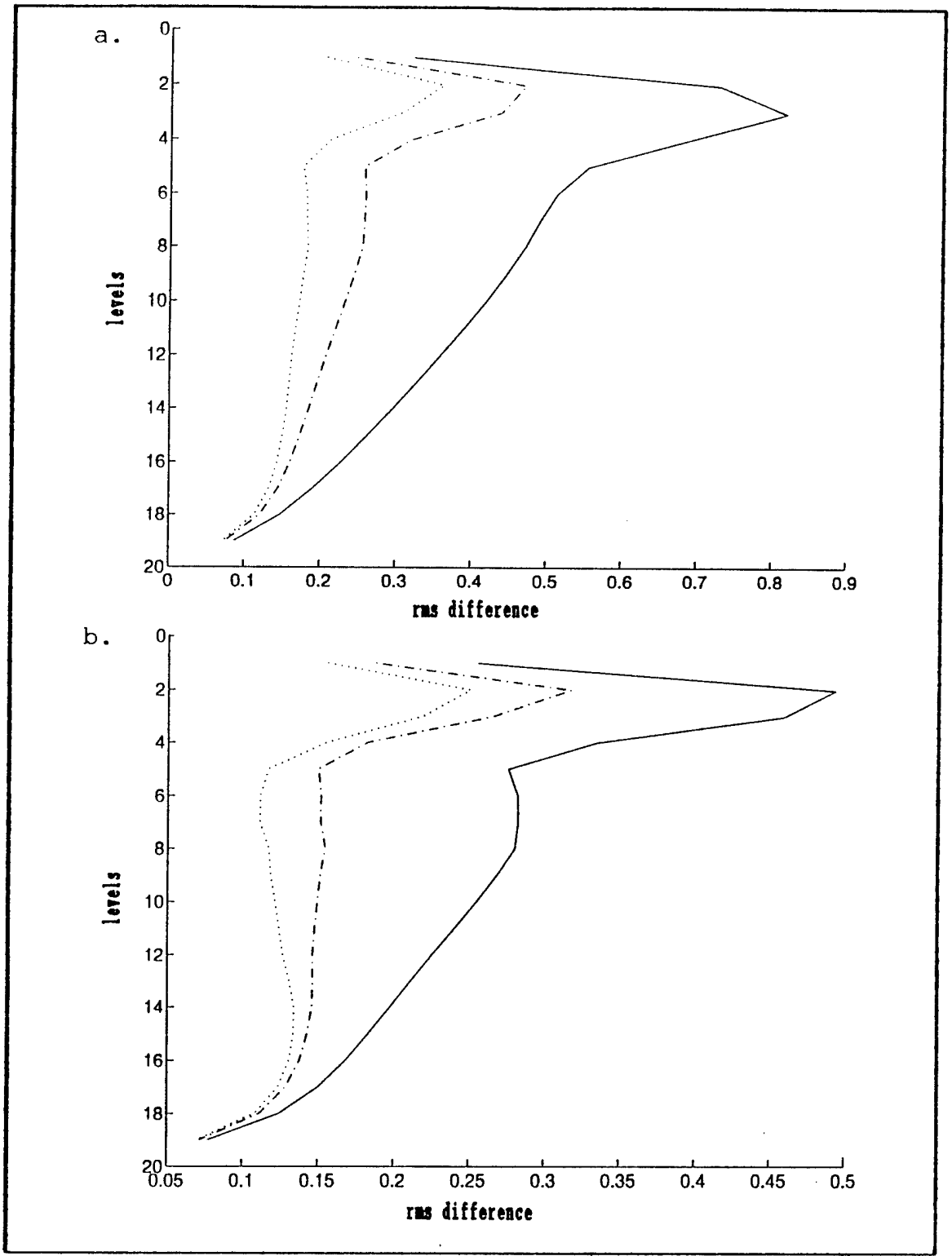

Figure 25. RMS of the Difference (m d^{-1}). (a) T = 9-hr. (b) T = 12-hr. Solid line, 1pass; dot dash line, 2pass; dot line, 3pass.

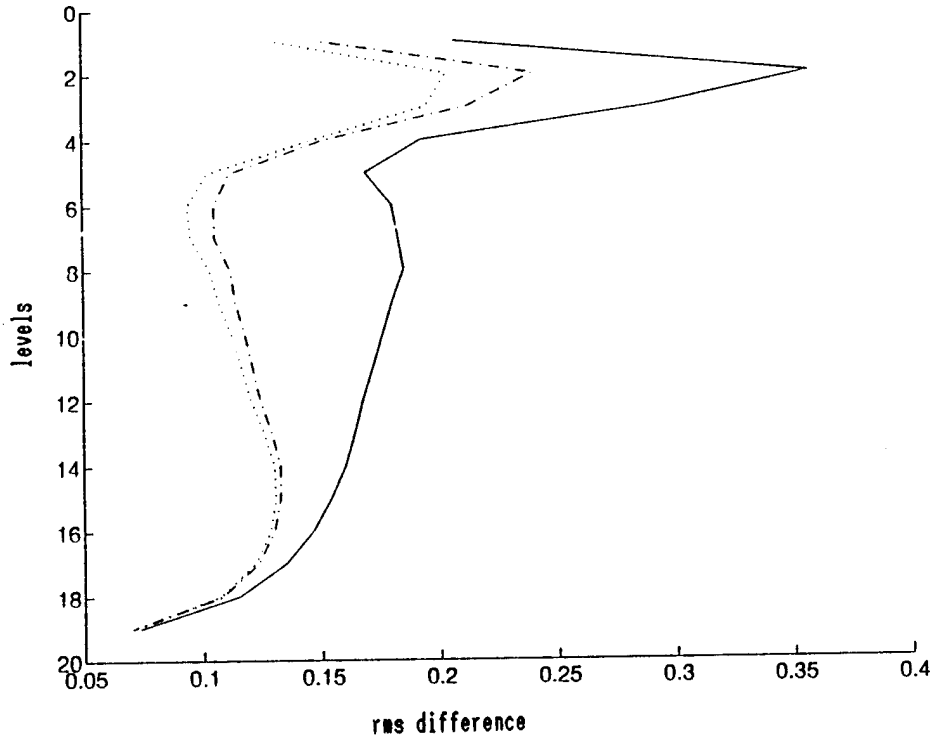

Figure 26. RMS of the Difference (m d^{-1}). T = 15-hr. Solid line, 1pass; dot dash line, 2pass; dot line, 3pass.

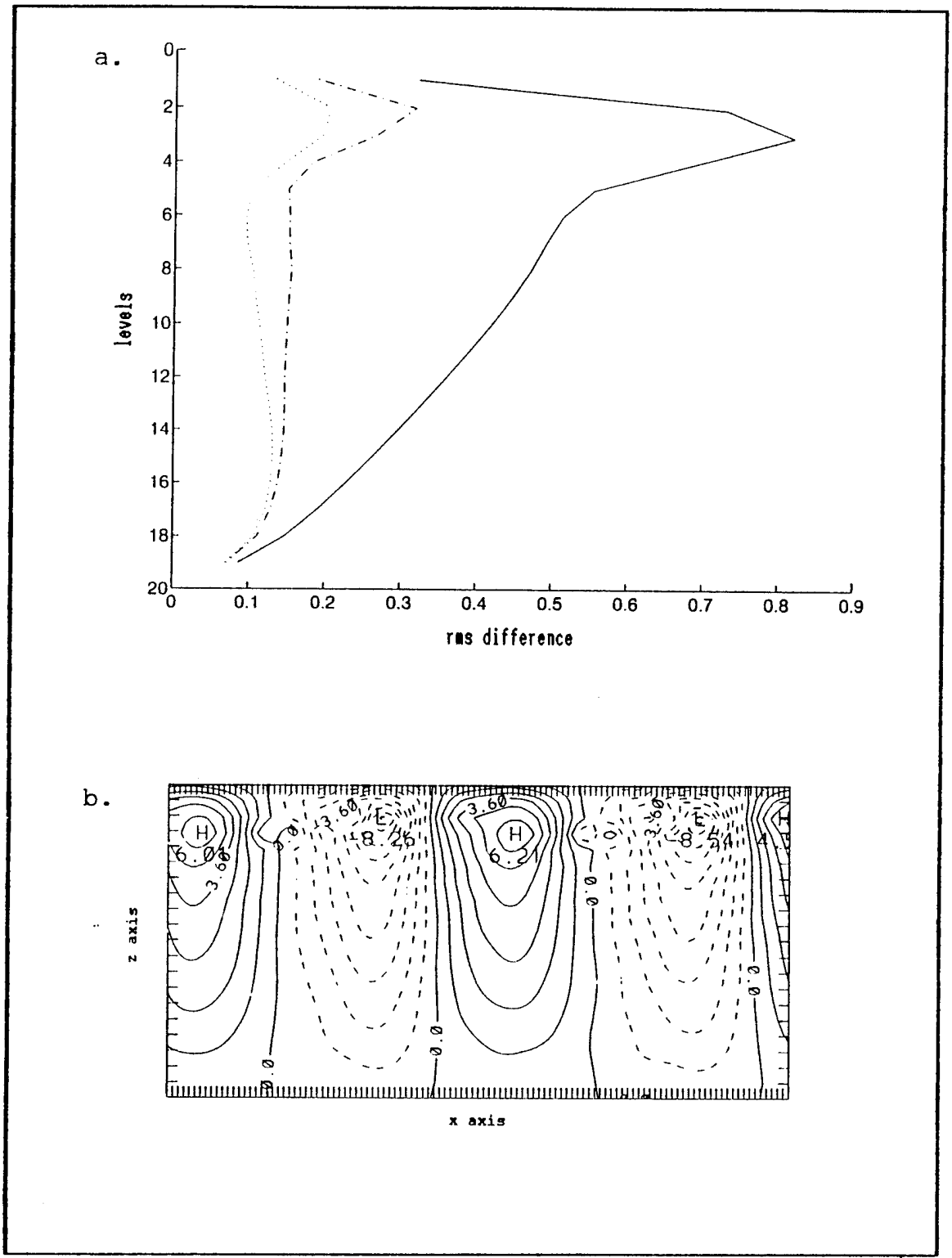

Figure 27. (a) RMS of the Difference combined plot (m d^{-1}). Solid line, 9-hr 1pass; dot dash line, 12-hr 2pass; dot line, 15-hr 3pass. (b) W vertical profile (m d^{-1}).

where the vertical velocities are large, but increases where the values of w are small (Figure 28).

Like the findings from the Rossby wave tests, the results show that the 12-hr and 15-hr integration times reproduce the control's currents the best. However, the increased computational time needed for the 15-hr DFI integration, does not produce a significantly smaller percent of error. Therefore, the DFI procedure with the 12-hr integration time and 3 passes is considered to give the best practical results.

The results show that the rms of the difference between vertical velocities is small for the 12-hr 3rd pass DFI method, at all model levels (Figure 29.a), and the normalized rms error is under 15% for all levels, except at the surface and the lowest five levels (2560 - 4000 m)(Figure 29.b, and Table II). This increased error near the top and bottom is most likely due to the lack of resolution in these regions and the adiabatic assumption of the DFI process. The conclusion is that the errors are acceptably small, and that the 12-hr 3rd pass DFI method returns the original values with highly useful accuracy as shown in Figures 24, and 30.

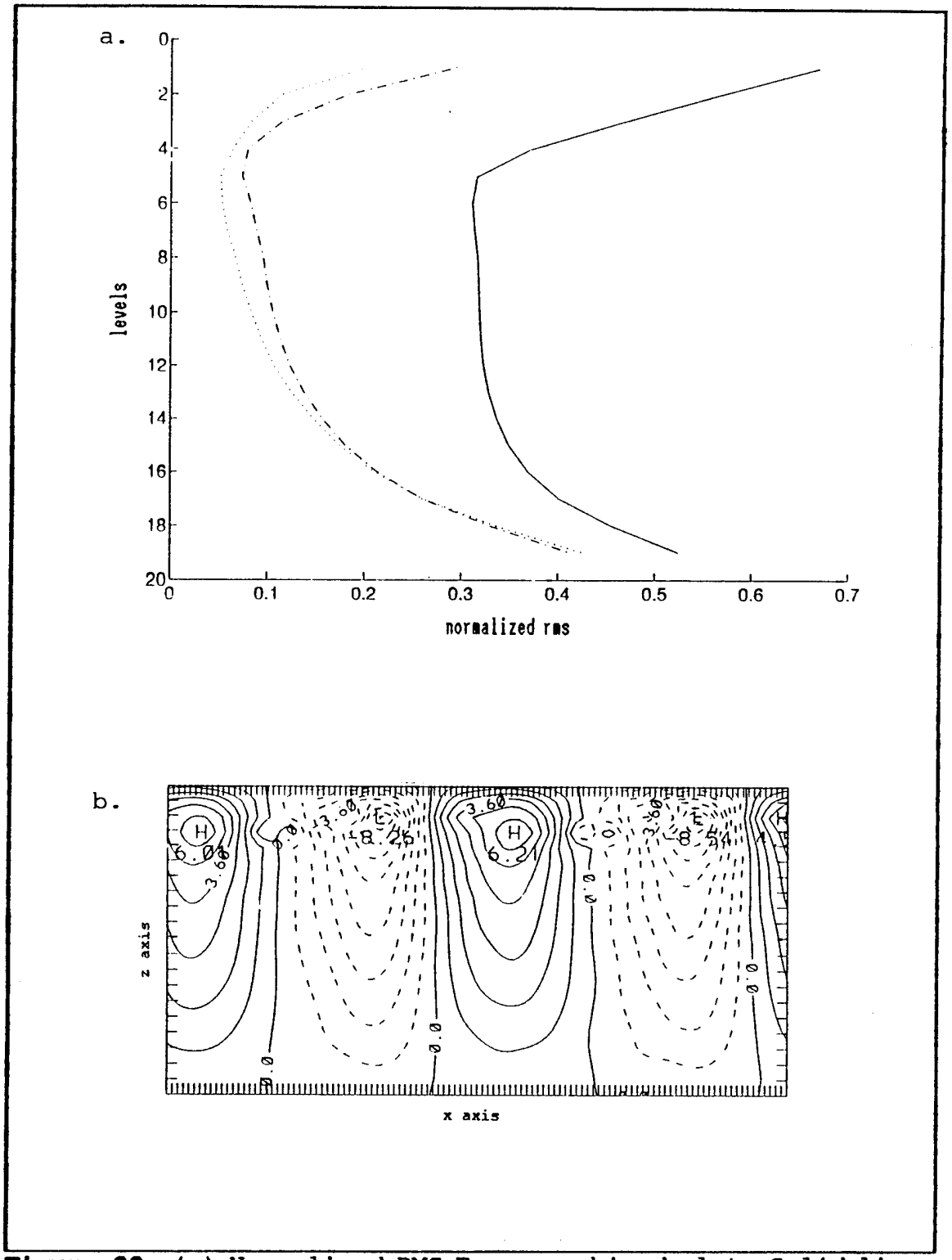

Figure 28. (a) Normalized RMS Error combined plot. Solid line, 9-hr 1pass; dot dash line, 12-hr 2pass; dot line, 15-hr 3pass. (b) W vertical profile (m d^{-1}).

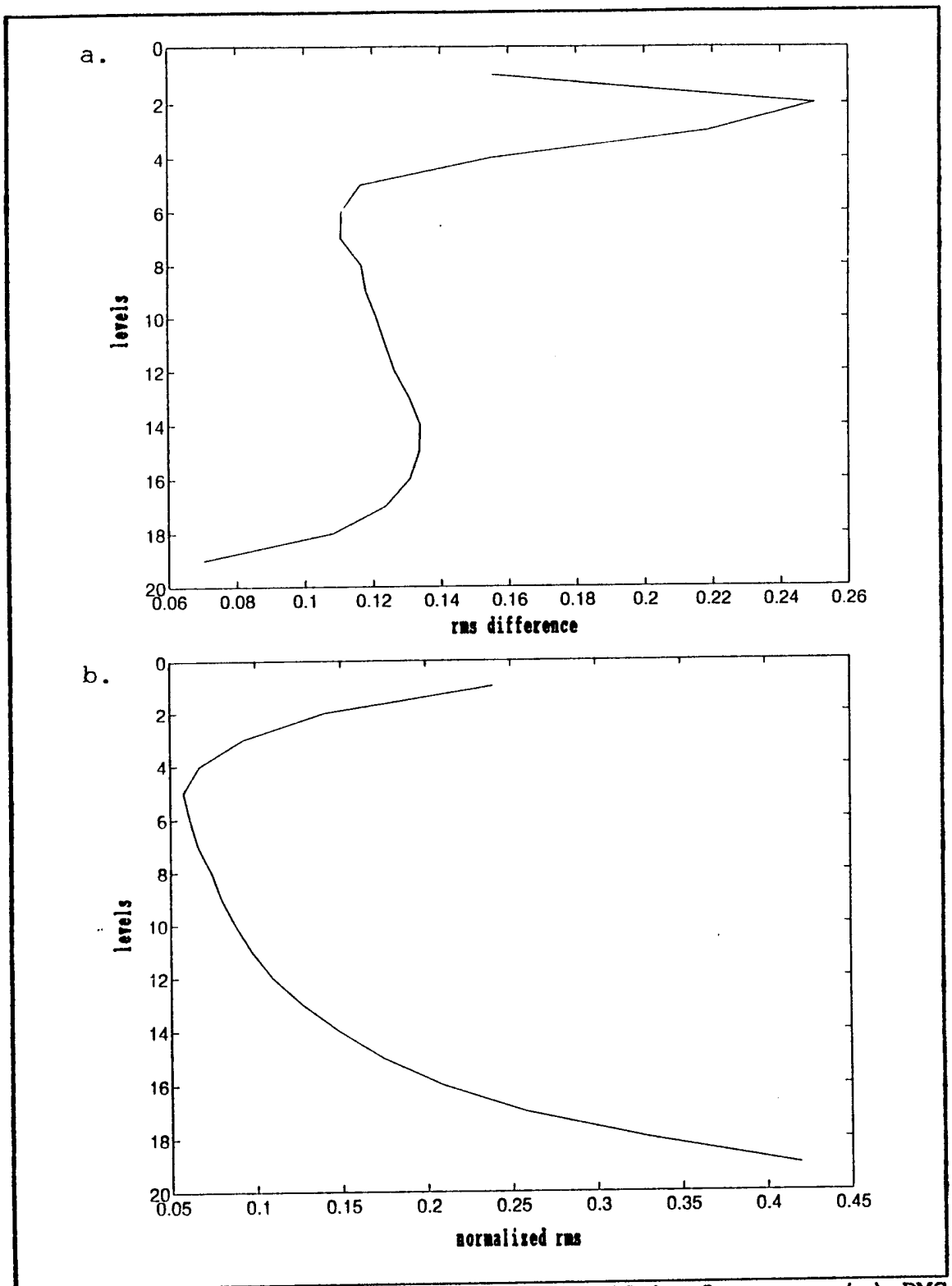

Figure 29. DFI Verification Using T = 12-hr 3passes. (a) RMS of the difference (m d^{-1}). (b) Normalized RMS error.

Baroclinic Unstable Flow:

T = 12-hr 3pass

Model Level	Depth (m)	RMS DIFFERENCE RMS($w - w_f$)	NRE RMS($w - w_f$) / RMS(w)
1	10	0.1553140	0.2397167
2	40	0.2500682	0.1408043
3	90	0.2185996	9.2744939 E-02
4	160	0.1549404	6.7110352 E-02
5	250	0.1165265	5.7649828 E-02
6	360	0.1109206	6.1324663 E-02
7	490	0.1107548	6.5937974 E-02
8	640	0.1167470	7.3884249 E-02
9	810	.01180682	7.9604834 E-02
10	1000	0.1211561	8.7748334 E-02
11	1210	0.1237135	9.7322747 E-02
12	1440	0.1264377	0.1095053
13	1690	0.1307218	0.1267268
14	1960	0.1338995	0.1484055
15	2250	0.1335814	0.1741401
16	2560	0.1308055	0.2089019
17	2890	0.1236864	0.2580079
18	3240	0.1082318	0.3314812
19	3610	7.0083916 E-02	0.4196966

Table II. Error Between Control and DFI w Velocities.

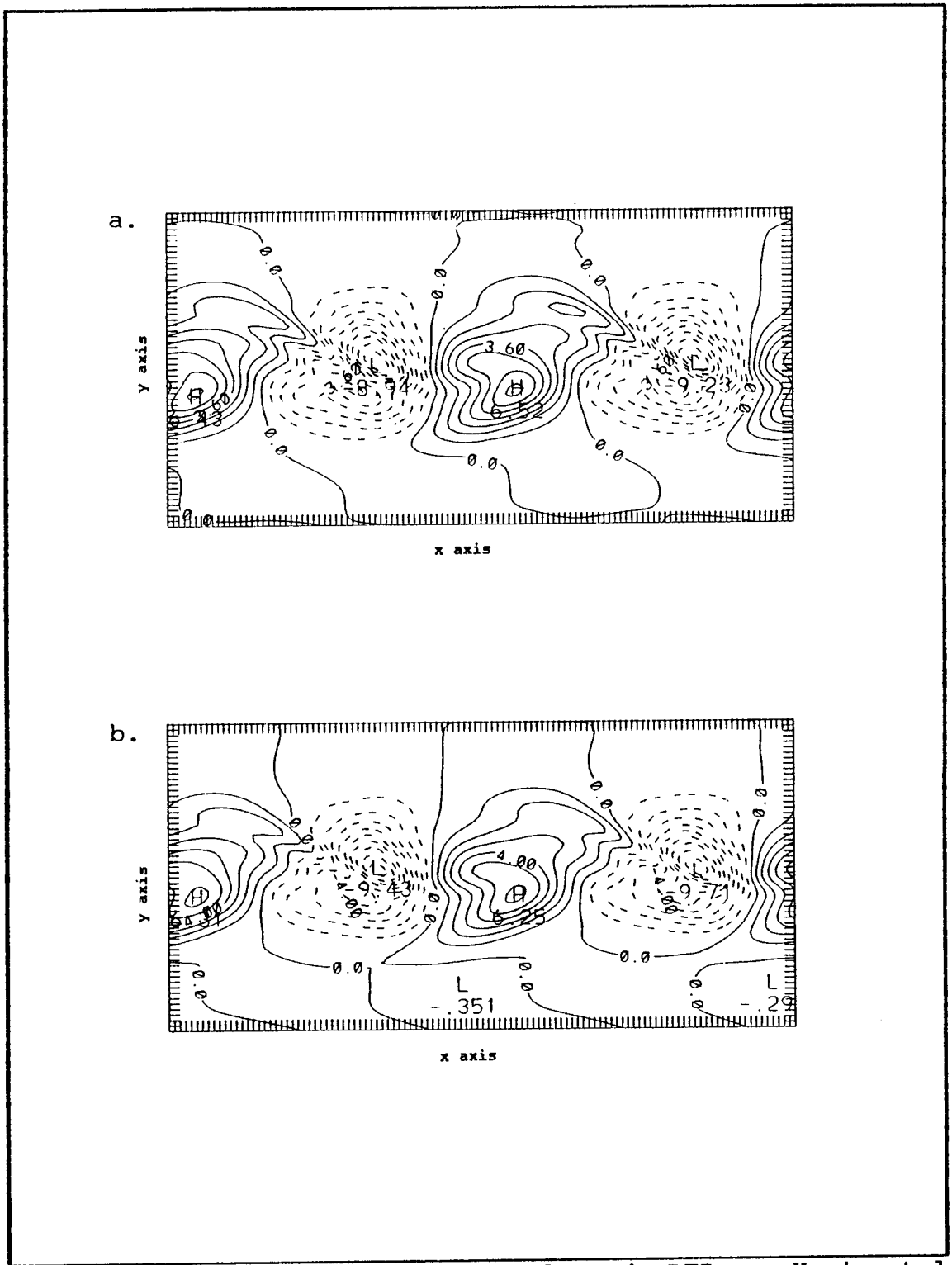

Figure 30. Comparison of Control and DFI w Horizontal Profiles, 90 m. (a) Control (m d^{-1}). (b) DFI, T = 12-hr 3passes (m d^{-1}).

III. DISCUSSION AND CONCLUSIONS

The DFI method was tested to see how accurately it could recover the three dimensional circulation from the initial density field and its geostrophic velocities alone. Two types of disturbances were used, a linear Rossby wave, and a finite amplitude disturbance growing on an unstable baroclinic flow. Four different integration times were used in the DFI procedure with the Rossby wave and three with the baroclinic unstable flow, all of which where repeated up to three times. The absolute error and the percent error for each time span and pass were calculated. These "measures of skill" were then compared to determine which best diagnosed the currents from the control run. Attention was focused on the vertical velocity because of its large signal and its dynamical importance.

In both test cases the 12-hr integration time with 3 passes produced the best practical results. Though there continued to be increases of accuracy at longer integration times, these were small enough to be confident that the 12-hr integration had recover the majority of the current. There were certain preferred areas that exhibited larger normalized rms errors (NRE ~ 0.3) in both cases.

The Rossby wave had increased normalized rms errors at the lower levels. This was thought to be the result of the friction term used in the control run, but not in the DFI. The DFI run was constrained to remain adiabatic because it could not include such a term in its backward integration. This produced a phase error between the control and the DFI, where the DFI was 60 - 70 degrees ahead of the control. New work by Lynch and Huang are removing the requirement for the backward integration by the use of new filters that would use only forward integration and still be able to pull the filtered fields back to t = o. This would remove the

requirement for an adiabatic process and allow friction to be included in the DFI method. The inclusion of the friction term would mean a more accurate diagnoses of the actual ocean environment, where friction is found not only at the fluid/solid interface (coastline and ocean floor), but also in the upper levels where the fluid/air interface occur with resulting mixing. For the Rossby wave the DFI returns the control currents with less than 10% error, except where noted. If the friction term is included, a 10% or less error should be extended to the total domain.

Another possible explanation for the error that is found at the lower levels in the domain, is that the stability there is almost zero which may hamper the geostrophic adjustment. If the lower levels are unable to adjust then no matter what fix is applied to the model, there will always remain some error. The baroclinic unstable flow had significant normalized rms errors both near the surface and at the lower levels. These errors could be the result of poor vertical resolution and/or be some of the same problems due to the adiabatic (frictionless) assumption in the DFI. The relatively poor resolution near the surface was induced by the shallow vertical structure of the density disturbance where only a few levels were able to resolve it. The lower level resolution error maybe the result of the larger spacing between the levels with depth. The error could also be the result of the frictionless DFI procedures, or the failure of the geostrophic adjustment process in the deep ocean where the stability is so weak. It is hoped that at least two of these errors can be reduced by increasing the vertical resolution, and by running the control without friction. This could be done simply by reducing the total model depth and removing the frictional component from the control run.

Despite these errors, the DFI method in fact returned the control's currents, including the secondary circulation and

vertical velocity, with a high degree of accuracy. What is significant is that the vertical velocity was accurately found by using only the density field, and that it was done quickly and simply. This has great implications to forecast models, because now all velocities can be accurately found for a given location which can then be used to initialize the model. Also the recovered velocities have had almost all high frequency noise removed, which reduces the problems that gravity waves have caused in forecast models in the past. By applying the DFI to these models it will increase the confidence of their results and increase the understanding and knowledge of the mesoscale features in the littoral zone.

LIST OF REFERENCES

Bower, A. S., 1989: Potential Vorticity Balances and Horizontal Divergence along Particle Trajectories in Gulf Stream Meanders East of Cape Hatteras. J. Phys. Oceanogr., 19, 1669-1681.

Brink, K. H., Beardsley, R. C., Niiler, P. P., Abbott, M., Huyer, A., Ramp, S., Stanton, T., and Stuart, D., 1991: Statistical Propertied of Near-Surface Flow in the California Coastal Transition Zone. J. Geophys. Res., 96(c8), 14693-14706.

Carlson, T. N., 1991: Mid-Latitude Weather Systems. Harper Collins Academic, NY, NY.

Dalton, J. H., Boorda, J. M., Mundy Jr, C. E., 1994: Forward...From The Sea. Washington, D.C.: U.S. Government Printing Office.

Dewey, R. K., Moum, J. N., Paulson, C. A., Caldwell, D. R.,and Pierce, S. D., 1991: Structure and Dynamics of a Coastal Filament. J. Geophys. Res., 96(c8), 14885-14908.

Holton, J. R., 1992: An Introduction To Dynamic Meteorology. Third edition, Academic Press, Inc., San Diego, CA.

Kadko, D. C., Washburn, L., and Jones, B., 1991: Evidence of Subduction Within Cold Filaments of the Northern California Coastal Transition Zone. J. Geophys. Res., 96(c8), 14909-14926.

Lindstrom, S. S., and Watts, D. R., 1994: Vertical Motion in the Gulf Stream Near 68° W. Paper submitted to J. Phys. Oceanogr.

Lorenz, E. N., 1992: The Slow Manifold--What Is It?. J. Atmos. Sci., 49, 2449-2451.

Lynch, P., and X. Y. Huang, 1992: Initialization of the HIRLAM Model Using a Digital Filter. Mon. Wea. Rev., 120, 1019-1034.

O'Keefe, S., Kelso III, F. B., Mundy Jr, C. E., 1992: ...From The Sea, Preparing the Naval Service for the 21st Century. Washington, D.C.: U.S. Government Printing Office.

Onken, R., 1992: Mesoscale Upwelling and Density Finestructure in the Seasonal Thermocline - A Dynamical Model. J. Phys. Oceanogr., 22, 1257-1273.

Paduan, J. D., and Niiler, P. P., 1990: A Lagrangian Description of Motion in Northern California Coastal Transition Filaments. J. Geophys Res., 95(c10), 18095-18109.

Pedlosky, J., 1964: An Initial Value Problem in the Theory of Baroclinic Instability. Tellus, 16, 12-17.

Strass, V. H., 1994: Mesoscale Instability and Upwelling. Part 2: Testing the Diagnostics of Vertical Motion with a Three-Dimensional Ocean Front Model. J. Phys. Oceanogr., 24, 1759-1767.

Swenson, M., Niiler, P., Brink, K., and McClain, E., 1992: Drifter Observation of a Cole Filament off Point Arena, California, in July 1988. J. Geophys. Res., 97(c3), 3593-3610.

Washburn, L., Kadko, D. C., Jones, B. H., Hayward, T., Kosro, P. M., Stanton, T. P., Ramp, S., and Cowles, T., 1991: Water Mass Subduction and the Transport of Phytoplankton in a Coastal Upwelling System. J. Geophys. Res., 96(c8), 14927-14946.

INITIAL DISTRIBUTION LIST

		No. Copies
1.	Defense Technical Information Center Cameron Station Alexandria, Virginia 22304-6145	2
2.	Library, Code 52 Naval Postgraduate School Monterey, California 93943-5101	2
3.	Oceanography Department Code OC/BF Naval Postgraduate School 833 Dyer Rd Rm 331 Monterey, CA 93943-5122	1
4.	Meteorology Department Code MR Naval Postgraduate School 589 Dyer Rd Rm 252 Monterey, CA 93943-5114	1
5.	Meteorology Department Code MR/HY Naval Postgraduate School 589 Dyer Rd Rm 252 Monterey, CA 93943-5114	1
6.	Meteorology Department Code MR/WU Naval Postgraduate School 589 Dyer Rd Rm 252 Monterey, CA 93943-5114	1
7.	LT David E. Otis 1408 Haslett Rd Haslett, MI 48840	2
8.	Commander Naval Meteorology and Oceanography Command 1020 Balch Boulevard Stennis Space Center, MS 39529-5005	1
9.	Commanding Officer Naval Oceanographic Office Stennis Space Center, MS 39529-5001	1

10. Commanding Officer 1
FLENUMMETOCCEN
7 Grace Hopper Ave. Stop 4
Monterey, CA 93943-5501

11. Officer In Charge 1
Naval Research Laboratory
Stennis Space Center, MS 39529-5004

12. Superintendent 1
Naval Research Laboratory
7 Grace Hopper Ave. Stop 2
Monterey. CA 93943-5502

13. Chief of Naval Research 1
800 N. Quincy Street
Arlington, VA 22217

14. Office of Naval Research 1
(Code 322)
Navy Ocean Modeling Program (NOMP)
800 N. Quincy Street
Arlington, VA 22217

15. Library 1
Department of Oceanography
University of Washington
Seattle, WA 98105

16. Library 1
College of Oceanography
Oregon State University
Corvallis, OR 97331

17. Director, Pacific Marine Center 1
(N/MOP)
National Ocean Service, NOAA
1801 Fairview Ave. East
Seattle, WA 98102

18. Chief, Ocean Services Division 1
National Oceanic and Atmospheric Administration
8060 Thirteenth Street
Silver Springs, MD 20910

19. NOAA Library 1
7600 Sand Point Way NE
Building 3
Seattle, WA 98115

20. Commanding Officer 1
Naval Research Laboratory
Washington, DC 20375-5000